Copper(II) Binding to Amyloid-β Fibrils of Alzheimer's Disease Reveals a Picomolar Affinity: Stoichiometry and Coordination Geometry Are Independent of Aβ Oligomeric Form

ARTICLE *in* BIOCHEMISTRY · APRIL 2009

Impact Factor: 3.02 · DOI: 10.1021/bi900254n · Source: PubMed

4 AUTHORS:

Claire Sarell
University of Leeds
10 PUBLICATIONS **287** CITATIONS
SEE PROFILE

Christopher Syme
University of Glasgow
23 PUBLICATIONS **1,018** CITATIONS
SEE PROFILE

Stephen E J Rigby
The University of Manchester
105 PUBLICATIONS **2,266** CITATIONS
SEE PROFILE

John H Viles
Queen Mary, University of London
49 PUBLICATIONS **3,295** CITATIONS
SEE PROFILE

4388 *Biochemistry* **2009,** *48,* 4388–4402
DOI:10.1021/bi900254n

BIOCHEMISTRY
including biophysical chemistry & molecular biology
Article

Copper(II) Binding to Amyloid-β Fibrils of Alzheimer's Disease Reveals a Picomolar Affinity: Stoichiometry and Coordination Geometry Are Independent of Aβ Oligomeric Form[†]

Claire J. Sarell, Christopher D. Syme, Stephen E. J. Rigby, and John H. Viles*

School of Biological and Chemical Sciences, Queen Mary University of London, Mile End Road, London E1 4NS, U.K.

Received February 16, 2009; Revised Manuscript Received April 1, 2009

ABSTRACT: Cu^{2+} ions are found concentrated within senile plaques of Alzheimer's disease patients directly bound to amyloid-β peptide (Aβ) and are linked to the neurotoxicity and self-association of Aβ. The affinity of Cu^{2+} for monomeric Aβ is highly disputed, and there have been no reports of affinity of Cu^{2+} for fibrillar Aβ. We therefore measured the affinity of Cu^{2+} for both monomeric and fibrillar Aβ(1−42) using two independent methods: fluorescence quenching and circular dichroism. The binding curves were almost identical for both fibrillar and monomeric forms. Competition studies with free glycine, L-histidine, and nitrilotriacetic acid (NTA) indicate an apparent (conditional) dissociation constant of 10^{-11} M, at pH 7.4. Previous studies of Cu-Aβ have typically found the affinity 2 or more orders of magnitude weaker, largely because the affinity of competing ligands or buffers has been underestimated. Aβ fibers are able to bind a full stoichiometric complement of Cu^{2+} ions with little change in their secondary structure and have coordination geometry identical to that of monomeric Aβ. Electron paramagnetic resonance studies (EPR) with Aβ His/Ala analogues suggest a dynamic view of the tetragonal Cu^{2+} complex, with axial as well as equatorial coordination of imidazole nitrogens creating an ensemble of coordination geometries in exchange between each other. Furthermore, the N-terminal amino group is essential for the formation of high-pH complex II. The Aβ(1−28) fragment binds an additional Cu^{2+} ion compared to full-length Aβ, with appreciable affinity. This second binding site is revealed in Aβ(1−42) upon addition of methanol, indicating hydrophobic interactions block the formation of this weaker carboxylate-rich complex. A Cu^{2+} affinity for Aβ of 10^{11} M^{-1} supports a modified amyloid cascade hypothesis in which Cu^{2+} is central to Aβ neurotoxicity.

Alzheimer's disease (AD)[1] is a progressive neurodegenerative disorder characterized by deposits of extracellular amyloid plaques in the brain. Amyloid-β peptide (Aβ) is 39−43 residues in length and is the main constituent of these deposits. Aβ is critical in the initial build up of these plaques (*1*); in particular, genetic alterations underlying familial AD are associated with mutations in Aβ or an increase in the production of Aβ(1−42) in the brain (*2*). The accumulation of amyloid plaques is fundamental to the pathology of AD, eventually swamping the extracellular interstitium of the brain. Studies on the neurotoxic element of Aβ suggest that small diffusible oligomers, or pore-forming protofibrils, rather than mature amyloid fibers may be the most toxic form, and these oligomers cause memory loss due to synapse failure (*3*).

Notable characteristics of AD are altered metal ion concentrations in the brain and disrupted metal ion homeostasis (*4*, *5*). Cu^{2+} levels in the AD neuropil are 400% higher than in the neuropil of a healthy brain, with Cu^{2+} and Zn^{2+} levels present in amyloid plaque deposits at 0.4 and 1 mM for Cu^{2+} and Zn^{2+}, respectively (*6*). Raman microscopy has provided direct evidence that copper and zinc are bound via the histidine imidazole rings of Aβ in isolated senile plaque cores (*7*). In addition, synchrotron X-ray fluorescence has identified hot spots in which Cu^{2+} and Zn^{2+} are concentrated within Aβ-associated amyloid plaques (*8*).

Normal levels of Cu^{2+} in the brain are more than sufficient to be neurotoxic if Cu^{2+} homeostasis and compartmentalization of Cu^{2+} are impaired (*9*, *10*). Oxidative damage is a key feature of the pathogenesis of AD (*11*), and the neurotoxicity of Aβ has been linked to H_2O_2 production (*12*). Cu^{2+} Fenton cycling is the probable source of reactive oxygen species (ROS) (*9*). Aβ chelation of Cu^{2+} may be a protective antioxidant response to oxidative stress (*13*, *14*), while diffusible oligomeric forms of Aβ may concentrate redox active Cu^{2+} at the neuronal membrane, causing lipid peroxidation (*13*, *15*). A recent key study shows transfer of copper from Aβ to a redox-inactive form bound to metallothionein negates Aβ's neurotoxic properties (*16*).

[†]This work was funded by Biotechnology and Biological Sciences Research Council project grants.

*To whom correspondence should be addressed. E-mail: j.viles@qmul.ac.uk. Telephone: (44) 020 7882 8443. Fax: (44) 020 8983 0973.

[1]Abbreviations: Aβ, amyloid-β peptide; AD, Alzheimer's disease; CD, circular dichroism; CSF, cerebrospinal fluid; cw-EPR, continuous wave electron paramagnetic resonance; EM, *N*-ethylmorpholine buffer; HEPES, *N*-(2-hydroxyethyl)piperazine-*N*′-2-ethanesulfonic acid; NTA, nitrilotriacetic acid; ThT, thioflavin T.

 Published on Web 4/1/2009

Soluble Aβ(1−40) and Aβ(1−42) are present in the cerebrospinal fluid (CSF) and blood plasma (*17*, *18*), but the trigger that promotes oligomerization and fibril formation is a subject of debate. Physiological levels of Cu^{2+} and Zn^{2+} will cause marked aggregation of Aβ (*19*−*21*), and while some studies suggest Zn^{2+} and Cu^{2+} promote amorphous aggregation of Aβ (*19*) but inhibit fibril formation (*22*, *23*), others have suggested fibril assembly occurs only in the presence of Cu^{2+} ions (*24*). Specific Cu^{2+} chelators can reverse the aggregation that occurs in AD and cause solubilization of amyloid deposits from post-mortem AD brain tissue (*25*), and thus Cu^{2+} chelators represent a possible therapy for Alzheimer's disease (*26*−*28*). Controversially, it has been shown that trace amounts of copper in a high-cholesterol diet induce amyloid plaques and learning deficits in a rabbit model of Alzheimer's disease (*29*, *30*).

We have previously described the characterization of Cu^{2+} binding to soluble Aβ(1−28) (the Cu^{2+} binding domain of Aβ) in aqueous solution (*31*) as well as a ^{1}H NMR study on Zn^{2+} binding to Aβ(1−28) (*32*). A number of biophysical techniques have been applied to probe the coordination geometry of monomeric Aβ and its metal coordinating fragments (for reviews, see ref *33* and in particular ref *34*). Recent studies include pulse EPR (*35*) (*36*) potentiometry (*37*) (*38*), extended X-ray absorption (*39*), and ^{1}H NMR (*40*). There are also data on the coordination of Cu^{2+} binding to Aβ(1−42) in its fibrillar form (*41*, *42*), although affinity- and pH-dependent Cu^{2+} coordination to Aβ fibrils has not been reported.

Potentially, the Cu^{2+} complex formed by Aβ in a fibrillar state may be very different from that formed by monomeric Aβ in solution. Current models of Aβ fibrils indicate in-register stacking of Aβ monomers (*43*). This causes histidine side chains (which have a high affinity for Cu^{2+} ions) at positions 13 and 14 to stack close together in successive peptides creating a possible Cu^{2+} coordination site containing four histidine residues. Thus, potentially, fibrils may be created or stabilized by inter-molecular histidines linking to each other via Cu^{2+} ions.

The affinity of Cu^{2+} for Aβ is key to its physiological significance, and there is certainly a need for further experimental data in this area. There are large discrepancies between the affinities reported for monomeric Aβ and no reports of affinities of Cu^{2+} for fibrillar Aβ. Dissociation constants for monomeric Aβ range from micromolar to nanomolar (*31*, *44*−*46*) and, in one report, up to attomolar [$K_d \sim 10^{-18}$ M (*47*)].

We use two independent techniques, fluorescence quenching and circular dichroism, to determine the Cu^{2+} affinity for fibrillar Aβ. We also determine both the stoichiometry and pH dependence of Cu^{2+} binding. EPR- and fluorescence-based affinity measurements are used to identify the ligands coordinating to the two Cu^{2+} ion binding sites within Aβ. This is achieved by the use of peptide analogues, in which the N-terminal amino group is acetylated or histidines are replaced with alanines.

EXPERIMENTAL PROCEDURES

Peptide Syntheses and Purification. Peptides representing various fragments of the amyloid-β peptide were synthesized by employing solid phase Fmoc chemistry and produced by the ABC facility at Imperial College (London, U.K.). After removal from the resin and deprotection, the samples were purified using reverse phase HPLC and characterized using mass spectrometry and ^{1}H NMR.

Design of Peptides. Peptides were synthesized of the human sequence of Aβ(1−40) and Aβ(1−42) in which the N-terminus and C-terminus were left as the native amino and carboxyl groups, respectively. In the fragments, the truncated C-terminus was blocked as the corresponding ethyl ester but Asp1 retains a free amino group. Together with the wild-type Aβ(1−28), four analogues of Aβ(1−28) were synthesized in which His6, His13, and His14 residues are replaced with alanine and one in which the N-terminus was acetylated, Aβ(Ac1−28). Two shorter fragments were also synthesized, Aβ(1−11) and Aβ(Ac10−16). Aβ(1−42); DAEFRHDSGYEVHHQKLVFFAEDVGSNKG AIIGLMVGGVVIA, Aβ(H6A); DAEFR**A**DSGYEVHHQKL VFFAEDVGSNK, Aβ(H13A); DAEFRHDSGYEV**A**HQKLV FFAEDVGSNK, Aβ(H14A); DAEFRHDSGYEVH**A**QKLV FFAEDVGSNK, Aβ(Ac1−28); Ac-DAEFRHDSGYEVHH QKLVFFAEDVGSNK, and Aβ(Ac10−16); Ac-YEVHHQK.

Solubilization of Aβ(1−40) and Aβ(1−42). Lyophilized full-length Aβ was solubilized at 0.7 mg/mL in water (ultra high quality, > 18 Ω cm resistivity) at pH 10.5 and gently rocked at 5 °C for a minimum of 48 h. To achieve minimal fibrillar content in the "monomeric Aβ", samples were freshly prepared from the pH 10.5 stock and spectral data immediately obtained. Although even freshly prepared Aβ may contain some dimers and low-molecular weight oligomers, thioflavin T (ThT) and CD measurements suggest no detectable fibrillar or β-sheet content in these samples.

Fibrillization of Aβ(1−42). The solubilized peptide (pH 10.5, 0.7 mg/mL) was diluted to 50 μM in the appropriate buffer, with 160 mM NaCl at pH 7.4. The peptide was then left for 72 h at 37 °C with agitation. Fibril growth was monitored and confirmed by the sigmoidal thioflavin T fibril growth curve as shown in Figure S1 of the Supporting Information. Conversion of irregular to high β-sheet content was detected by UV circular dichroism. Furthermore, fibril content was confirmed by seeding studies, in which small aliquots of Aβ deemed to be fibrillar and added to monomeric Aβ reduced the lag phase of fibril growth curves by typically 10 h, to less than 30 min. In addition, transmission electron microscopy (TEM) with uranyl acetate staining indicates characteristic fibril morphology.

Titrations. Peptide concentrations were determined using an extinction coefficient of 1280 M^{-1} cm^{-1} (due to the single tyrosine residue) at 280 nm (*48*). Typically, the freeze-dried peptides contained ∼10% moisture by weight. UV−visible electronic absorption spectra were recorded with a Hitachi U-3010 double-beam spectrophotometer, using a 1 cm path length quartz cuvette.

The pH was measured before and after each spectrum was recorded. Ten millimolar phosphate buffer, 10 mM *N*-ethylmorpholine (EM) buffer, and 10 mM *N*-(2-hydroxyethyl)piperazine-*N*′-2-ethanesulfonic acid (HEPES) were used in the EPR pH dependence study. Typically, unless otherwise stated, 10 mM phosphate buffer with 160 mM NaCl (pH 7.4) was used for most experiments except for the affinity studies which were typically performed in the absence of buffer, ultra high quality (> 18 Ω cm resistivity) water with 160 mM NaCl (pH 7.4). The pH was adjusted using small amounts of 10−100 mM NaOH or HCl. The addition of metal ions or competing ligands to the Aβ peptides was performed using small aliquots from stock aqueous solutions (10−50 mM) of $CuCl_2$, glycine, L-histidine, or nitrilotriacetic acid (NTA), obtained from Sigma Aldrich, analar grade or better.

EPR. X-Band electron paramagnetic resonance (EPR) data were recorded using a Bruker ELEXSYS 500 spectrometer,

operating at a microwave frequency of ~9.3 GHz. Spectra were recorded using a microwave power of 4.012 mW across a sweep width of 2000 G (centered at 3200 G) with a modulation amplitude of 7 G. Samples were frozen in quartz tubes and experiments conducted at typically 20 K using a liquid helium cryostat. A minimum of four scans were recorded per spectrum. All EPR spectra shown have been background subtracted from a buffer blank with subsequent baseline correction in the EPR software package using third- or fourth-order polynomial splines. To analyze EPR data using the method described by Peisach and Blumberg (*49*), it is necessary to convert values from gauss (G) to millikaysers (mK) by using the formula $A_{\|}$ (mK) = $0.046686g\Delta H$, where $g = 2.0023$ and ΔH is the $A_{\|}$ splitting measured in gauss. Double integration was carried out on the signal between 3200 and 3400 G to determine signal intensity.

Circular Dichroism (CD). CD spectra were recorded on a Chirascan (Applied Photophysics) circular dichroism spectrometer at 25 °C. A 1 cm path length was used for data between 300 and 800 nm, and a 0.1 cm path length was used for the far-UV data. A minimum of three scans were recorded for all spectra, including baseline spectra, which were subtracted from each spectrum. Applied Photophysics Chirascan Viewer was used to apply minimal smoothing to the data if required. The Kaleidagraph spreadsheet/graph package was used to present data. Direct CD measurements (θ, in millidegrees) were converted to molar ellipticity, $\Delta\varepsilon$ (M^{-1} cm^{-1}), using the relationship $\Delta\varepsilon = \theta/(33000cl)$, where c is the concentration and l the path length.

Fluorescence Spectroscopy. Fluorescence spectra were collected using a Hitachi F-2500 fluorescence spectrophotometer. For tyrosine quenching studies, an excitation frequency of 280 nm was used and data were collected between 290 and 400 nm. Samples were placed in a 1 cm quartz cuvette (Hellma) and data recorded at room temperature. For fibril growth studies using ThT, an excitation wavelength of 444 nm was used and data were collected over the range of 455−520 nm with an average of three scans and gentle magnetic stirring. Additionally, measurements with a BMG Fluostar Galaxy multiwell plate reader were used to provide confirmation of the fibril growth curve in Figure S1a of the Supporting Information.

Affinity Measurements. Stability constants for Cu^{2+} bound to competitive ligands nitrilotriacetic acid (NTA), histidine, and glycine are as follows. The absolute affinity (pH-independent) of NTA for Cu^{2+} is 1.26×10^{13} M^{-1} (*50*); the apparent affinity, at pH 7.4, is therefore 5.0×10^{10} M^{-1} or a dissociation constant of 19.9 pM (as $\log \alpha = pK_a - pH = 9.8 - 7.4 = 2.4$ and $\log K_1(app)$ at pH 7.4 = $\log K_1 - \log \alpha = 13.1 - 2.4 = 10.7$). Histidine and glycine form a $Cu(His)_2$ and $Cu(Gly)_2$ complex, and the affinities are given by K_1 and K_2 respectively (*50*), for example, as $K_{d1}K_{d2} = [Cu_{free}][Gly_{free}]^2/[Cu(Gly)_2]$. Apparent dissociation constants (K_{d1} and K_{d2}) at pH 7.4 are 1.35 and 13.5 μM for glycine and 3.7 nM and 0.47 μM for histidine, respectively. The absolute affinities for NTA, histidine, and glycine are given alongside apparent affinities at pH 7.4 in Figure S2 of the Supporting Information.

The Cu^{2+}:Aβ stoichiometry for full-length Aβ is shown to be 1:1. The fraction of Cu^{2+} bound to Aβ (θ) was calculated assuming this relates directly to the fraction of fluorescence tyrosine signal quenched by Cu^{2+} (dynamic scattering is taken to be minimal). Indeed, addition of Cu^{2+} to Aβ causes a linear reduction in the magnitude of the fluorescence signal up to 1 molar equiv of Cu^{2+} ions. The affinity can thus be calculated from the fluorescence at half the maximal value. Under these conditions ($\theta = 0.5$), the dissociation constant $K_d = [Cu^{2+}_{free}]$. By free Cu^{2+}, we mean Cu^{2+} not bound to Aβ or the competing ligand. The value of $[Cu^{2+}_{free}]$ is given by eq 1 for NTA, which forms only a 1:1 complex with Cu^{2+}, or given by eq 2 for glycine and histidine (*46*).

$$[Cu^{2+}{}_{free}] = \frac{1}{1 + K_{a1}[NTA]}([Cu^{2+}{}_{total}] - [Cu^{2+}{}_{bound\ to\ A\beta}]) \quad (1)$$

$$[Cu^{2+}{}_{free}] = \frac{1}{1 + K_{a1}[Gly] + K_{a1}K_{a2}[Gly]^2}([Cu^{2+}{}_{total}] - [Cu^{2+}{}_{bound\ to\ A\beta}]) \quad (2)$$

Alternatively, the K_d at pH 7.4 of Aβ for Cu^{2+} can also be calculated from the observed K_d in the presence of the competing ligand glycine by using eq 3 (*51*).

$$K_d = K_d(\text{observed in the presence of Gly}) \times \frac{K_{d1}(\text{apparent for Gly})}{[\text{total Gly}]} \times \frac{K_{d2}(\text{apparent for Gly})}{[\text{total Gly}]} \quad (3)$$

RESULTS

Affinity of Cu^{2+} Binding. The affinity of Cu^{2+} for Aβ is vital in understanding the physiological significance of Cu^{2+} in Alzheimer's disease. There are currently conflicting experimental data for the affinity of binding of Cu^{2+} to monomeric Aβ and no data on the affinity of Cu^{2+} for fibrillar Aβ. To determine if the large (11 orders of magnitude) differences in Cu^{2+} binding to Aβ reported (*31*, *47*) might reflect the difference in the affinity of Cu^{2+} for different oligomeric forms of Aβ, two independent methods were used to measure the affinity of Cu^{2+} for both monomeric and fibrillar Aβ.

The competitive effects of glycine, L-histidine, and NTA were used to measure Cu^{2+} affinity for both monomeric and fibrillar Aβ(1−42) by fluorescence spectroscopy. Figure 1a shows that the addition of increasing amounts of Cu^{2+} to Aβ(1−42) causes marked quenching of the single tyrosine (Tyr10) fluorescence signal at 307 nm. It is notable that tyrosine fluorescence spectra of fibers give a fluorescence intensity generally comparable to that of monomeric Aβ at 50 μM. A plot of fluorescence versus molar equivalents of Cu^{2+} (Figure 1a inset) indicates a linear reduction in fluorescence for addition of up to 1 molar equiv of Cu^{2+}. By 1 molar equiv of Cu^{2+}, the fluorescence intensity is reduced by ~75%. A break point at 1 molar equiv indicates 1:1 stoichiometry, as continued addition of Cu^{2+} causes only a slight further reduction in fluorescence attributed to nonspecific interaction of Cu^{2+} with the tyrosine (data not shown). The 1:1 stoichiometry is confirmed by EPR studies (Figures 6 and 7).

Figure 1b shows the effect of glycine addition on a 1:1 Cu−Aβ complex. As glycine is added, it competes with Aβ for the Cu^{2+} ions and the tyrosine fluorescence signal at 307 nm reappears. The maximum tyrosine fluorescence signal, for both soluble and fibrillar Aβ, returns only after more than 200 molar equiv of glycine has been added. Half the maximal quenching is achieved at 55 molar equiv of glycine for soluble Aβ(1−42), and similarly 56 molar equiv for fibrillar Aβ(1−42). Free glycine will bind to

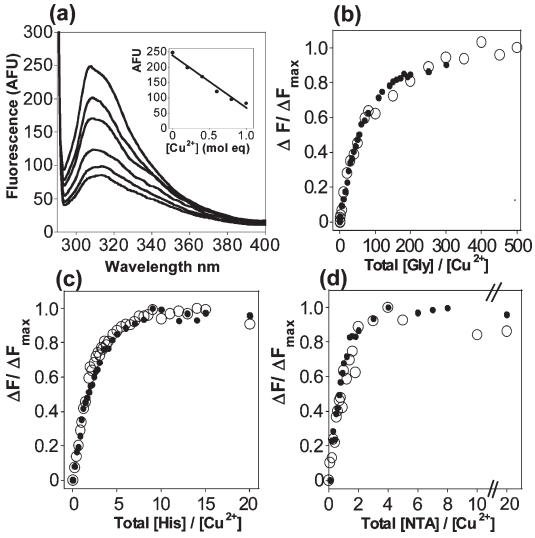

FIGURE 1: Fluorescence spectra of monomeric and fibrillar Aβ(1−42) with Cu^{2+}: glycine, L-histidine, and NTA competition. (a) Increasing additions of Cu^{2+} (0.2, 0.4, 0.6, 0.8, and 1.0 molar equiv) to 50 μM Aβ(1−42) in water at pH 7.4 causes quenching of the tyrosine fluorescence signal. The tyrosine fluorescence signal at 307 nm returns with additions of molar equivalents of glycine (b), L-histidine (c), or NTA (d). Monomeric Aβ(1−42) (●) and fibrillar Aβ(1−42) (○) with 50 μM Cu^{2+} present. $\Delta F = F - F_o$, and $\Delta F_{max} = F_{max} - F_o$, where F_o is the fluorescence (307 nm) with addition of 1 molar equiv of Cu^{2+}.

Cu^{2+} ions in a $Cu(Gly)_2$ complex, coordinating via the amino and carboxylate groups. The stepwise apparent affinity for glycine is known: $K_{a1} = 7.4 \times 10^5$ M^{-1}, and $K_{a2} = 7.4 \times 10^4$ M^{-1} at pH 7.4 (*50*) (see Table S2 of the Supporting Information). It is sometimes not appreciated that the affinity of glycine for Cu^{2+} is the product of the affinities of K_1K_2 and related to $[Gly]^2$ (see Experimental Procedures). The apparent dissociation constant for the Cu−Aβ complex at pH 7.4 may be calculated using eq 2 (Experimental Procedures and Supporting Information). Using this method, we calculated K_d values at pH 7.4 of 58 and 60 pM for both monomeric and fibrillar Aβ(1−42), respectively. Identical values are calculated using the alternative approach in eq 3 (see Experimental Procedures and calculations in the Supporting Information).

The experiment was then repeated using either competing ligand L-histidine or NTA, each of which has a higher affinity for Cu^{2+} than glycine (Figure 1c,d). NTA has an apparent dissociation constant for Cu^{2+} at pH 7.4 of 19.9 pM (*50*) and binds Cu^{2+} to form a 1:1 complex, making determination of the K_d more straightforward. It is clear from Figure 1d that addition of 1 molar equiv of NTA removes just more than half the Cu^{2+} from Aβ, indicating that Cu^{2+} has a very similar affinity for Aβ as NTA (20 pM). Using eq 1 and the concentration of NTA added at half the maximal fluorescence (0.70 molar equiv), we can calculate the dissociation constant at pH 7.4 for monomeric Aβ(1−42). An apparent K_d of 14 pM is determined, which is within the same order of magnitude as that determined using glycine as the competitive ligand.

L-Histidine is known to bind Cu^{2+} with stepwise apparent K_d values at pH 7.4 of 3.7 nM (K_{d1}) and 0.47 μM (K_{d2}). Two molecules of histidine will bind a single Cu^{2+} ion using the amino and imidazole nitrogens as ligands. The tyrosine fluorescence signal at 307 nm returns to its maximum value for both soluble and fibrillar Aβ after only 5 molar equiv of L-histidine has been added, as shown in Figure 1c. Half-maximal quenching is achieved at close to 1.7 molar equiv for soluble Aβ(1−42) and 1.5 molar equiv for fibrillar Aβ. This is below the 2 molar equiv of histidine required to bind 1 molar equiv of Cu^{2+} and indicates that Cu^{2+} will bind to Aβ(1−42) with an affinity comparable to that of L-histidine. Again, the affinity can be calculated using eq 2, this time using the K_{a1} and K_{a2} values of histidine at pH 7.4 and the concentration of histidine at half-maximal quenching. The histidine competition experiment indicates an apparent dissociation constant of 6 pM for monomeric and 8 pM for fibrillar Aβ at pH 7.4. Again, these values are similar to those calculated using NTA as the competing ligand. Although there is some variation, the K_d values are within a single order of magnitude, between 6 and 60 pM.

Importantly, we have obtained similar affinities of Cu^{2+} for Aβ with a second independent method using near-UV CD spectroscopy. These near-UV experiments have an advantage in that they measure a CD signal directly associated with the Cu−Aβ complex. Figure 2 shows the CD spectrum of Aβ(1−28) loaded with 1 molar equiv of Cu^{2+} ions at pH 7.4. We have previously shown that although the Cu−Aβ complex does not give rise to CD bands for d−d electronic transitions, there is a positive CD band at 320 nm assigned to Aβ−Cu imidazole charge transfer transitions (*31*). This CD band increases in intensity with addition of Cu^{2+}. Figure 2 shows that as the competing ligand NTA is added the intensity of the band decreases. A plot of ellipticity at 320 nm, shown as an inset, indicates the band is reduced to half its maximal intensity only after 0.75 molar equiv of NTA is added. The binding curve using NTA as a competitor bears a striking resemblance to the NTA competition studies using fluorescence quenching shown in Figure 1d. Like the fluorescence data, the CD data indicate Cu^{2+} has an affinity for Aβ similar to that of NTA, i.e., 20 pM. A similar experiment was performed using glycine. Here the intensity of the Cu−Aβ CD bands at 320 nm was reduced to half the maximal intensity at ca. 35 molar equiv of glycine. Using eq 2 or 3, we calculate the apparent Cu^{2+} dissociation constant for Aβ(1−28) at pH 7.6 to be 110 pM. This value is comparable to a K_d of 90 pM determined using glycine competition and fluorescence quenching of Aβ(1−28) at pH 7.8. It was not possible to repeat this experiment for Aβ(1−42) as the CD band at 320 nm was not of sufficient intensity.

In summary, using both direct measurements of Cu^{2+} from CD bands of the Cu−Aβ complex and fluorescence quenching methods, we have shown that 1 molar equiv of Cu^{2+} ions binds to Aβ(1−42) with a dissociation constant similar to that of NTA. An apparent conditional K_d at pH 7.4 between 6 and 60 pM for Aβ(1−42) is calculated. Significantly, comparisons of Aβ(1−40) and Aβ(1−42) in the monomeric and fibrillar forms show almost identical affinity for a single Cu^{2+} ion at pH 7.4.

pH Dependence of Cu^{2+} Binding. We were interested in how the Cu−Aβ(1−42) coordination changes with pH. Preliminary studies suggested that the choice of buffer affected the pH dependence behavior. EPR spectra of monomeric Aβ(1−42) loaded with 1 molar equiv of Cu^{2+} ions were therefore obtained over a range of pH values under four different sample conditions: 10 mM HEPES, 10 mM ethylmorpholine (EM), 10 mM phosphate buffer, or just water (as shown in Figure 3 and Figure S3 of the Supporting Information). It is notable that repeat EPR (or CD) scans recorded over time showed no change in the appearance of the spectra, indicating Cu^{2+} coordination to Aβ reaches a thermodynamic equilibrium rapidly, within minutes.

The EPR spectrum at pH 5 for the Cu−Aβ(1−42) complex under all four buffer conditions gives a single set of signals typical of type II Cu^{2+}, square-planar or square pyramidal coordination geometry, as shown in Figure 3a. Regardless of the buffer, the $A_{\|}$, $g_{\|}$, and $g_{\perp}$ values are 171 G (16.0 mK), 2.27, and 2.02, respectively (designated complex I). At pH 7.4, a new set of hyperfine peaks can be observed at a higher field with $A_{\|}$, $g_{\|}$, and $g_{\perp}$ values of 154 G (14.4 mK), 2.23, and 2.01, respectively (designated complex II), as shown in Figure 3b. At pH 7.4, complex I remains the more intense of the two under all four conditions, and notably in water, phosphate, or HEPES buffer, ca. 80% of the Cu^{2+} forms complex I. At pH 9 (Figure 3c), the low- and high-field sets of signals of complexes I and II are of comparable intensity in water, phosphate buffer, and HEPES buffer. However, for ethylmorpholine buffer (EM), the low-field species observed exclusively at pH 5 is considerably less intense than the high-field species. The relative intensities of the two complexes are shown in Figure 3 d−f. The pH dependence of the formation of complexes I and II is very similar for phosphate, water, and HEPES (Figure 3d,e) with a midpoint of pH ~9; however, the midpoint in EM buffer (Figure 3f) is lower at pH 8.0.

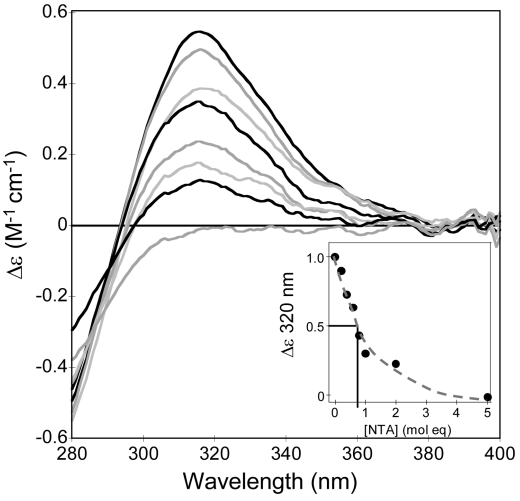

FIGURE 2: CD spectra of Aβ(1−28) with Cu^{2+} assessed via NTA competition. Increasing molar equivalents of NTA added to 50 μM Aβ(1−28) and 50 μM Cu^{2+} causes a decrease in the intensity of the CD signal at 320 nm. The inset shows the normalized CD signal at 320 nm of the Cu^{2+}−Aβ(1−28) complex with increasing molar equivalent additions of NTA.

This behavior is also observed for Aβ(1−28) as shown in Figure S3 of the Supporting Information. Comparison of EPR spectra for Aβ(1−28) and Aβ(1−42) shows a close correspondence at all pH values. The midpoint of the transition for Aβ(1−28) was pH ~9, similar to that for Aβ(1−42), and again, in EM buffer this was reduced to pH 8.0.

The effect of EM buffer on the midpoint of transition between complexes I and II was unexpected as EM has a very low affinity for Cu^{2+} ions. Buffers can have a temperature dependence to their pH. A recent study has shown that the pH of some buffers can vary by as much as 1 pH unit between room temperature and 10 K (liquid helium temperatures) (*52*) (*53*). This may well account for the discrepancies between EM buffer and the other buffers tested.

Peisach and Blumberg have shown that a combination of $A_{\|}$ and $g_{\|}$ values can indicate the ligand type that coordinates the

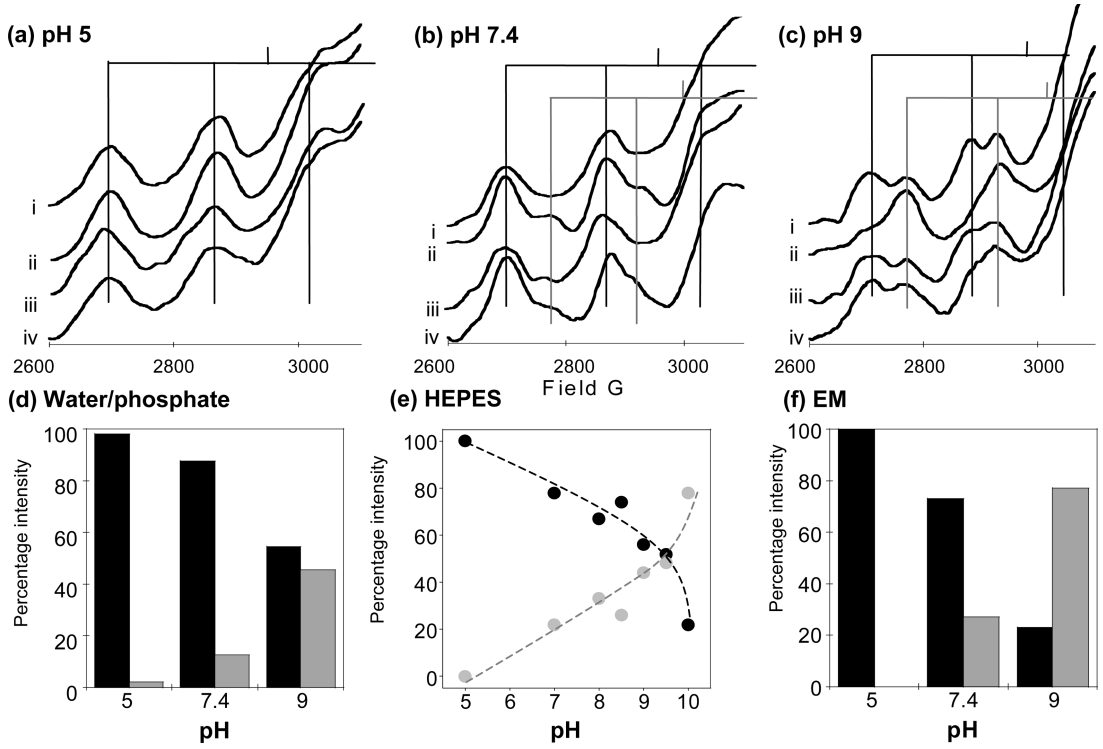

FIGURE 3: pH and buffer dependence of Cu^{2+} binding to monomeric Aβ(1−42). Cu EPR spectra of 50 μM Aβ(1−42) with 1 molar equiv of Cu^{2+} at (a) pH 5.0, (b) pH 7.4, and (c) pH 9.0. Spectra were recorded in four different buffering conditions at each pH: (i) water, (ii) 10 mM ethylmorpholine, (iii) 10 mM phosphate, and (iv) 10 mM HEPES. Plots d−f show relative percentage intensities of EPR signals from complex I (low pH) (black bars) and complex II (high pH) (gray bars), specifically in water and phosphate buffer (average values used as both buffers produced almost identical spectra) in panel d, while plot e shows 10 mM HEPES buffer (black circles for complex I and gray circles for complex II) and in EM buffer (f). All samples contained 160 mM NaCl and were examined at 20 K. The midpoint of the transition between complex I and II is pH ~9 for water, HEPES, and phosphate buffer but pH 8.0 for EM.

Table 1: $A_{\|}$ and $g_{\|}$ for Aβ Fragments and Analogues and Dissociation Constants

	complex I (pH 7.4)		complex II (pH 9)		
peptide	$A_{\|}$	$g_{\|}$	$A_{\|}$	$g_{\|}$	K_d
Aβ(1−42) mono	16.0 mK (171 G)	2.27	14.4 mK (154 G)	2.23	58 pM[a]
Aβ(1−42) fibrillar	16.0 mK (171 G)	2.27	not measured		60 pM[a]
Aβ(1−28) WT	15.9 mK (170 G)	2.27	14.7 mK (156 G)	2.22	90 pM,[b] 110 pM[c]
Aβ(1−28) NB	15.7 mK (168 G)	2.29	not present		750 pM[b]
Aβ(1−28) H6A	15.7 mK (168 G)	2.28	15.8 mK (169 G)	2.22	237 pM[b]
Aβ(1−28) H13A	15.3 mK (164 G)	2.28	15.1 mK (162 G)	2.22	128 pM[b]
Aβ(1−28) H14A	15.5 mK (166 G)	2.28	15.6 mK (167 G)	2.22	128 pM[b]
Aβ(10−16)	16.7 mK (178 G)	2.26	not present		3.1 nM[b]
Aβ(1−11)	13.6 mK (146 G)	2.30	not measured		−
Aβ(1−28) 2nd molar equiv	16.4 mK (175 G)	2.28	not measured		−

[a] Apparent (conditional) dissociation constants taken from Gly competition fluorescence quenching data at pH 7.4. For NTA and His competition 14 and 6 pM was determined respectively. [b] Denotes a K_d at pH 7.8; raw data previously reported (*31*). [c] Denotes the K_d at pH 7.6 has been calculated using glycine competion and near-UV CD.

Cu^{2+} in tetragonal/square-planar complexes (*49*). The $A_{\|}$ and $g_{\|}$ values at pH 5 (summarized in Table 1) are most typical of two nitrogen and two oxygen ligands (2N2O), although 3N with 1O coordination cannot be ruled out. The $A_{\|}$ and $g_{\|}$ values of the high-field species that can be observed at pH 7.4 and 9 do not fall into the standard Peisach and Blumberg plot areas, suggesting some distortion in the axial plane (perhaps suggesting a more square pyridamal character), but are shifted away from the oxygen boundaries, suggesting a probable 3N1O or 4N coordination.

Comparison of Monomeric and Fibrillar Aβ. The in-register stacking of Aβ monomers in amyloids has raised the possibility that the Cu^{2+} coordination formed with amyloid fibers could be very different from the coordination with Aβ monomers. Figure 4 compares the EPR spectra of both monomeric and fibrillar Aβ loaded with 1 molar equiv of Cu^{2+} ions. It is clear almost identical EPR line shapes are obtained for the fibrillar and monomeric forms of Aβ(1−42), as shown in Figure 4a. Of particular note is the fact that there is no detectable line broadening of the fibrillar form compared to monomeric Aβ. EPR spectra reveal a type II axial coordination with an $A_{\|}$ of 16.0 mK (171 G) and a $g_{\|}$ of 2.27 which are typical for a 3N1O or 2N2O complex at pH 7.4. There are no significant differences in the hyperfine splitting between monomeric and fibrillar Aβ, and $A_{\|}$ and $g_{\|}$ are the same for both forms of Aβ.

It is notable that Cu^{2+} addition has little detectable effect on the secondary structure of fibers once formed, as determined by UV CD. The CD spectra of fibers are dominated by a strong negative band at 217 nm, indicative of β-sheet. The appearance of the spectra is unaffected by the addition of up to 15 molar equiv of Cu^{2+} ions as shown in Figure 4c.

To see if the oligomeric state of Aβ affects the Cu^{2+} coordination environment, Cu^{2+} was added to Aβ at different times during Aβ fibril growth (rather than present throughout) (Figure 4b). By monitoring growth using ThT fluorescence (shown in Figure S1 of the Supporting Information), we could obtain an estimate of the degree of oligomerization at different time points (*54*). At zero days, fresh Aβ represents the largely monomeric form of Aβ(1−42), with a very weak ThT fluorescence signal. The Aβ(1−42) species at 3 days represents early fibers, while 8 days represents more mature fibers. Again, the spectra are almost identical for all three forms of Aβ.

Cu^{2+} Coordination Ligands of Aβ(1−28) and Analogues [Aβ(H6A), Aβ(H13A), Aβ(H14A), Aβ(Ac1−28), and Aβ(Ac10−16)] and Their pH Dependence. To identify the residues directly involved in the coordination of Cu^{2+}, five peptide analogues have been synthesized. In three analogues of Aβ(1−28), one of the three histidines has been replaced with an alanine residue, Aβ(H6A), Aβ(H13A), and Aβ(H14A). An additional peptide has also been synthesized in which the N-terminus of Aβ(1−28) is blocked by acetylation. Under physiological conditions, it is believed that nitrogens from these four loci (the three imidazole rings and the N-terminal amino group) are the most likely candidates for Cu^{2+} coordination. Comparisons of EPR spectra by ourselves, and previously by Karr et al. (*65*), confirm that Aβ(1−28) contains all the ligands involved in coordinating the first molar equivalent of Cu^{2+} in Aβ(1−42). Finally, a shorter fragment, Aβ(Ac10−16), was also studied in which His6 and the N-terminal amino group are absent.

The cw-EPR spectra of all five analogues with 1 molar equiv of Cu^{2+} added were obtained over a range of pH values to probe the nature of the coordinating ligands and are shown in Figure 5. The Cu^{2+} complex for each analogue was studied at pH 5, 6, 7, 8, 9, and 10. All spectra indicate axial Cu^{2+} coordination containing N and O ligands. All but two of the analogues produced two sets of axial peaks.

At pH 5, only one set of $A_{\|}$ and $g_{\|}$ values is present in all five peptide analogues. All have an appearance similar to that of the low-pH species described for Aβ(1−28), Aβ(1−40), and Aβ(1−42). There are, however, subtle variations in the appearance of the spectra. The $A_{\|}$ and $g_{\|}$ values for the five peptides and wild-type Aβ are given in Table 1. All fall within a small range of $A_{\|}$ values between 170 and 164 G for complex I (predominant at pH 5 and 7.4) except for Aβ(Ac10−16) which has a larger $A_{\|}$ of 178 G. The $g_{\|}$ of complex I ranges from 2.26 for Aβ(Ac10−16) to 2.29 for N-terminally acetylated Aβ(Ac1−28).

Also shown in Table 1 are the affinities of Cu^{2+} for the Aβ analogues studied. These data are obtained from fluorescence quenching experiments previously reported (*31*). Here, we use the glycine concentration at half-maximal quenching to calculate dissociation constants at pH 7.8 using eq 2. It is notable that all analogues have reduced affinity for Cu^{2+} ions, indicating that all four nitrogen ligands identified have a role in stabilizing the Cu^{2+}−Aβ complex. The N-terminally blocked and His6Ala analogues show the most marked reduction in affinity, while H13A and H14A show less pronounced change in affinity for Cu^{2+} ions relative to wild-type Aβ(1−28).

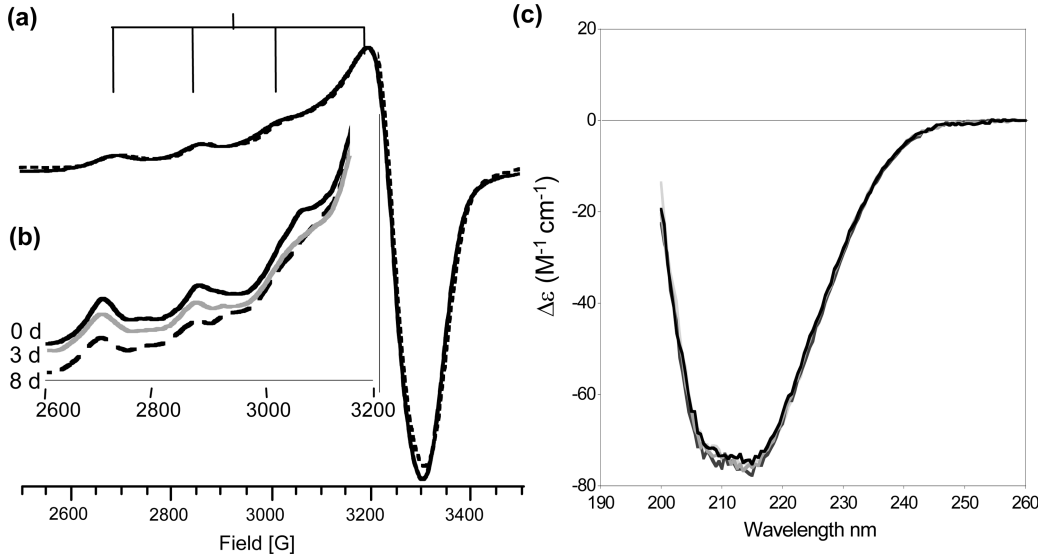

FIGURE 4: Cu^{2+} and different oligomeric species of Aβ(1−42). (a) EPR spectra of monomeric (dashed line) and fibrillar (solid line) Aβ(1−42) at 50 μM with 50 μM Cu^{2+} in 10 mM phosphate buffer with 160 mM NaCl at pH 7.4 and 20 K. Inset b shows additions of Cu^{2+} to 50 μM Aβ(1−42) after incubation for 0, 3, and 8 days. The Cu^{2+} coordination for monomeric and fibrillar Aβ is strikingly similar. Panel c shows a UV CD spectra of the predominantly β-sheet Aβ(1−40) fibrils with the addition of up to 15 molar equiv (750 μM) of Cu^{2+}.

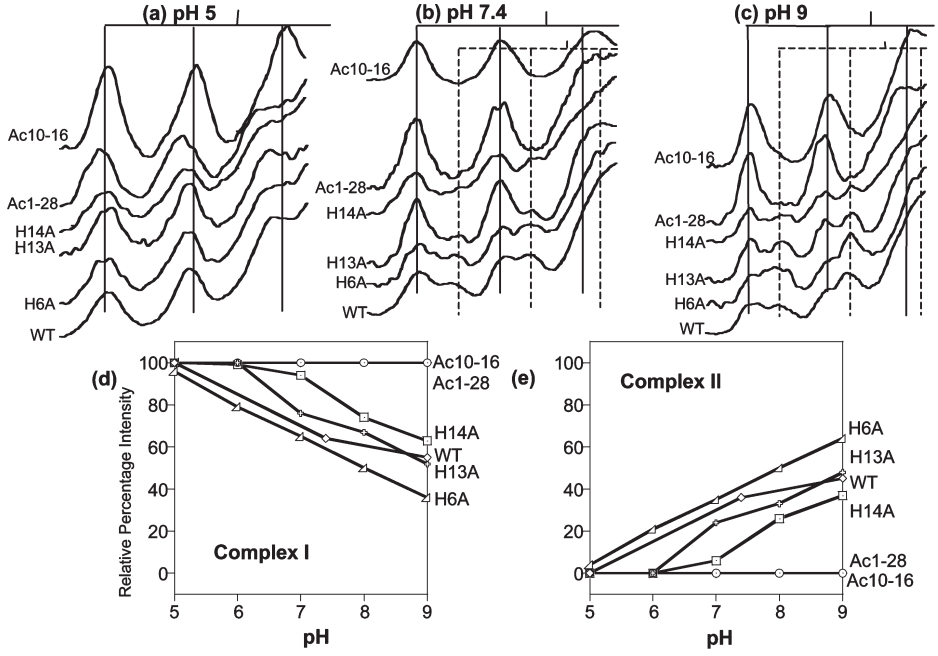

FIGURE 5: Cu^{2+} pH dependence of Aβ(1−28) analogues. Cu EPR spectra of Aβ(Ac10−16), Aβ(Ac1−28), Aβ(H6A), Aβ(H13A), Aβ(H14A), and Aβ(1−28) wild type at 50 μM with 1 molar equiv of Cu^{2+} at (a) pH 5, (b) pH 7.4, and (c) pH 9. Panels d and e show the relative percentage intensities of complex 1 (d) and complex 2 (e) of the six peptides over a wider range of pH values. It is clear the N-terminally acetylated analogues will not form high-pH complex II.

As the pH is increased to pH 7.4, the appearance of the EPR spectra differs between the analogues. A second, higher-field species is obtained for the Aβ(1−28) wild-type sequence and all the His-substituted analogues, with $A_{\|}$ and $g_{\|}$ values of ~165 G (15.4 mK) and 2.22, respectively, but significantly, it is not apparent in N-terminally acetylated analogue Aβ(Ac1−28) or Aβ(Ac10−16). Furthermore, the relative intensities of the two species are different between the analogues. The pH dependencies for complexes I and II are plotted as relative intensity versus pH for the five analogues and compared to that of wild-type Aβ(1−28), as shown in Figure 5d,e.

At pH 9, the high-field species (complex II) have an intensity similar to or greater than that of the low-field species for wild-type Aβ(1−28), H6A, and H13A, but for H14A, ~60% remains as component I and there is still no observable signal for the higher-pH complex II spectra in the N-terminally acetylated analogues.

In summary, all the peptide analogues have slightly different $A_{\|}$ and $g_{\|}$ values (summarized in Table 1) and perturbed pH dependencies compared to those of wild-type Aβ(1−28). In addition, all analogues have reduced affinity for Cu^{2+} ions (Table 1). Most striking are N-terminally blocked analogues, Aβ(Ac1−28) and Aβ(Ac10−16), both of which will not form complex II even at pH 9.

Stoichiometry of Cu^{2+} Binding. The process of fibril formation could lead to an intermolecular Cu^{2+} complex; for example, fibrillar Aβ might potentially form a 1:2 Cu(Aβ)$_2$ complex. To identify any differences in Cu^{2+} binding stoichiometry for monomeric and fibrillar forms of Aβ(1−42) and Aβ(1−40), EPR spectra were obtained with increasing molar equivalents of Cu^{2+} at pH 7.4 (shown in Figures 6 and 7). Increasing amounts of Cu^{2+} added to monomeric Aβ (Figure 6) gave identical line shapes up to 1 molar equiv, with a commensurate increase in intensity indicating a single binding mode. Titration of an additional 1 molar equiv of Cu^{2+} (and up to 10 molar equiv) results in no further increase in the intensity of the EPR spectra for either Aβ(1−40) or Aβ(1−42) in its monomeric form. This was a surprise as previous studies within our laboratory on Aβ(1−28) reported a 2:1 stoichiometry, two Cu^{2+} ions binding a single Aβ(1−28) molecule (*31*). Spin integration of the EPR spectra has been plotted versus Cu^{2+} addition as shown in Figure 6b. Both Aβ(1−40) and Aβ(1−42) show a linear increase in intensity up to 1 molar equiv of Cu^{2+} ions followed by saturation of the signal. The clear break point at 1 molar equiv of Cu^{2+} indicates that at 50 μM Aβ Cu^{2+} binds tightly to Aβ with a 1:1 stoichiometry. It should be noted that free Cu^{2+} ions in water at neutral pH give a largely EPR silent signal (*55*). This observation was confirmed by obtaining EPR spectra of 50 μM $CuCl_2$ in EM, PB, HEPES, and water buffer at pH 7.4 which showed that Cu^{2+} EPR signals are drastically attenuated relative to those of Cu^{2+} bound to Aβ.

We were then interested in the binding of Cu^{2+} to the fibrillar form of Aβ(1−40) and Aβ(1−42), as shown in Figure 7. Cu^{2+} binding curves (Figure 7c,d) for fibrillar Aβ(1−40) and Aβ(1−42) also show a maximal Cu^{2+} EPR signal at 1 molar equiv. After 1 molar equiv of Cu^{2+}, both Aβ(1−40) and Aβ(1−42) in their fibrillar form became saturated with Cu^{2+} at physiological pH. Because of the necessity of the long incubation of Aβ(1−42) at 37 °C, 0.05% (v/v) sodium azide was added to some samples; this had no effect on the stoichiometry or the $g_{\|}$ value, although $A_{\|}$ was reduced by approximately 2 G. Aβ(1−42) shows a slight reduction in the magnitude of the signal with further Cu^{2+} addition (> 1 molar equiv) due to some precipitation (~20%) of the less soluble Aβ(1−42) prior to freezing. As with monomeric Aβ, the EPR data indicate fibrillar Aβ(1−40) and Aβ(1−42) also bind a single Cu^{2+} ion. This is in contrast to the shorter soluble Cu^{2+} binding fragment Aβ(1−28). To further investigate this difference and to determine whether the hydrophobic tail of Aβ(1−42) was blocking the second Cu^{2+} binding site, methanol, an intramolecular hydrogen bond promoter, was added.

Stoichiometry of Cu^{2+} Binding: Effect of Methanol on the Hydrophobic Tail. The addition of 20% (v/v) methanol has a profound influence on increasing the stoichiometry of full-length Aβ. It is clear from the Cu^{2+} binding curve in Figure 8a that Aβ(1−42) has a 2:1 stoichiometry in the presence of methanol ions rather than the 1:1 stoichiometry observed in 100% water. As a direct comparison, Aβ(1−28) was also studied in 20% (v/v) methanol (Figure 8b); however, this had no effect on the binding stoichiometry, and Aβ(1−28) still bound two Cu^{2+} ions both with and without 20% (v/v) methanol present. The EPR spectra for the Cu^{2+}−Aβ complex in methanol or water are identical to those of the Cu^{2+}−Aβ complex in water alone.

We studied the effect of methanol on the secondary structure of monomeric Aβ(1−42) by UV CD. Measurements indicated no significant change in secondary structure from the peptide's random coil conformation with addition of 20% methanol

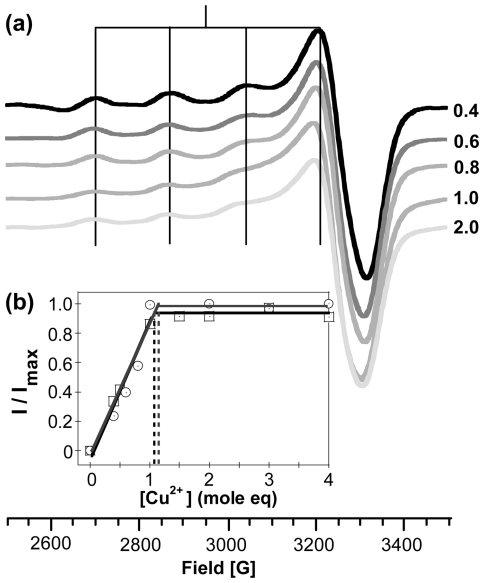

FIGURE 6: Cu^{2+} titration of monomeric Aβ(1−42). (a) EPR spectra recorded with 0.4, 0.6, 0.8, 1.0, and 2.0 molar equiv of Cu^{2+} and 50 μM Aβ(1−42) in 10 mM phosphate buffer at pH 7.4 and 20 K. Double integration of the EPR spectra of monomeric Aβ(1−40) (○) and Aβ(1−42) (□) with an increasing number of molar equivalents of Cu^{2+} is shown in panel b. Best fit straight lines are fitted through data points for 0−1 molar equiv of Cu^{2+} and 1−4 molar equiv of Cu^{2+}. The EPR signal intensity is I/I_{max}. Both monomeric Aβ(1−40) and monomeric Aβ(1−42) give a clear break point at 1 molar equiv of Cu^{2+} ions, indicating saturation of Aβ has occurred.

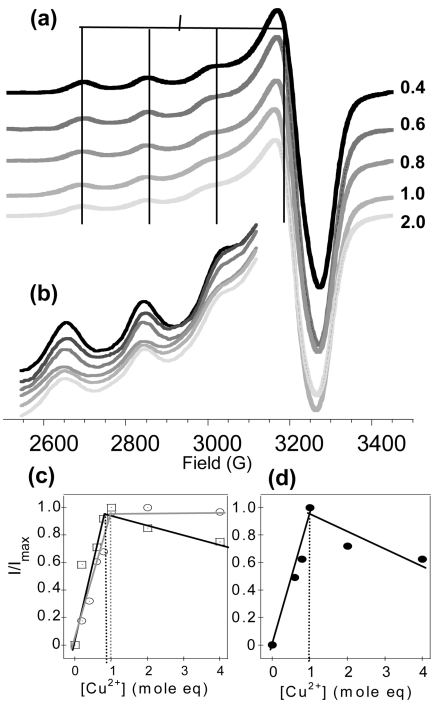

FIGURE 7: Cu^{2+} titration of fibrillar Aβ(1−42). (a) Increasing number of molar equivalents of Cu^{2+} with 50 μM Aβ(1−42) in phosphate buffer solution (up to 2 molar equiv at pH 7.4 and 20 K). (b) Hyperfine splitting showing the $A_{\|}$ of fibrillar Aβ(1−42). Panel c shows the double integration of the EPR spectra of fibrillar Aβ(1−40) with sodium azide (○) and fibrillar Aβ(1−40) with no sodium azide (□). Panel d shows the double integration of fibrillar Aβ(1−42) with no sodium azide (●) plotted vs molar equivalents of Cu^{2+} ions. All indicate that saturation occurs at 1 molar equiv of Cu^{2+}.

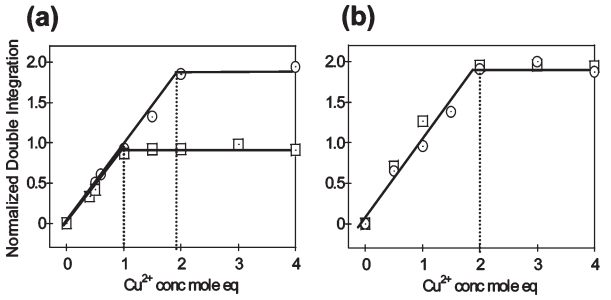

FIGURE 8: Effect of methanol on Aβ(1−42) stoichiometry. (a) Double integration of Aβ(1−42) in 100% water (□) and a water/methanol mixture (80:20, v/v) (○). (b) Double integration of Aβ(1−28) with (○) and without (□) 20% methanol. The Cu^{2+}−Aβ(1−42) complex undergoes a change in stoichiometry from 1:1 to 2:1 in the presence of methanol. The Cu^{2+}−Aβ(1−28) complex retains 2:1 stoichiometry irrespective of the presence of methanol. The concentration of Aβ(1−42) and Aβ(1−28) was 50 μM.

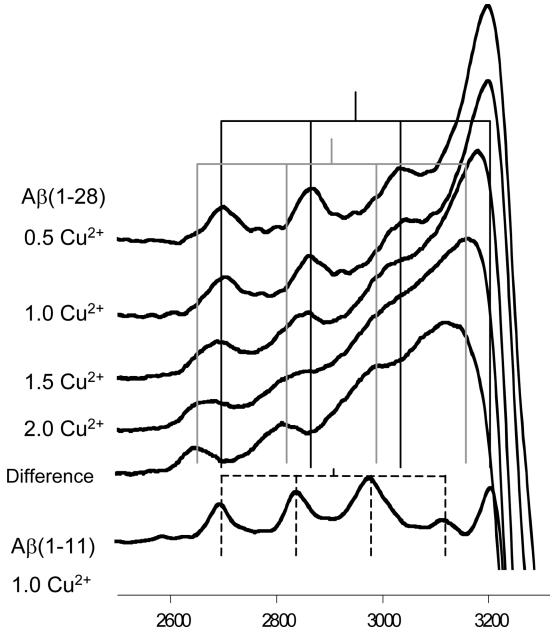

FIGURE 9: Comparison of the second Cu^{2+} binding site with Aβ(1−11). Aβ(1−28) with 0.5, 1.0, 1.5, and 2.0 molar equiv of Cu^{2+} present. The difference spectrum is the 2 molar equiv spectrum minus the 1 molar equiv spectrum. The difference spectra highlight the 3O1N nature of the second binding site which is very different from that of Aβ(1−11). See Table 1 for $A_{\|}$ and $g_{\|}$ values.

(Figure 4a of the Supporting Information). The affinity of the complex in 20% methanol was also measured using fluorescence with L-His as a competing ligand (Figure 4b of the Supporting Information). The half-maximal quenching occurs at close to 3 (~3.25) molar equiv of L-His for soluble Aβ(1−42) in 20% methanol, which is comparable to that for soluble Aβ without methanol.

Cu^{2+} Binding of the Second Molar Equivalent to Aβ. We were also interested in probing the nature of the binding site for the second molar equivalent of copper bound to Aβ(1−28). Figure 9 shows EPR spectra of 1 and 2 molar equiv of Cu^{2+} ions bound to Aβ(1−28), at pH 7.4. As we titrate Cu^{2+} beyond 1 equiv, a new set of signals appear to low field, while signals for the first equivalent of Cu^{2+} remain unaffected. A difference spectrum of Cu_2Aβ(1−28) minus Cu_1Aβ(1−28) is shown, emphasizing the appearance of the new set of signals at 2 molar equiv of Cu^{2+}. The copper type II spectrum gives $A_{\|}$ and $g_{\|}$ values of 16.36 mK (175 G) and 2.28, respectively. These values are more typical of an oxygen-rich complex such as 1N3O.

We were interested in the possibility that this second, weaker binding site originates from ligands found in the first 11 residues of Aβ. Thus, for the sake of comparison, an EPR spectrum of Aβ(1−11) with 1 molar equiv of Cu^{2+} added is also shown in Figure 9. It is clear that the weaker second binding site does not, in fact, mimic binding to the Aβ(1−11) fragment, which has $A_{\|}$ and $g_{\|}$ values of 144 G (13.6 mK) and 2.30, respectively, typical of 2N2O. Indeed, the spectra of the weaker second binding site do not resemble EPR spectra of any of the analogues studied (Table 1).

Temperature Dependence of Cu^{2+}−Aβ EPR: A Bridging Cu−His−Cu Dimer Is Unlikely. It has previously been suggested that there is histidine bridging two Cu^{2+} ions in the Aβ complex (*56*, *57*). We repeated this study using precisely the same conditions used by Smith et al. (*57*). However, we did not observe any line broadening to the spectra, shown in Figure S5 of the Supporting Information. EPR spectra in which electron coupling is taking place are very temperature-dependent and will be effectively decoupled at lower temperatures (20 K) (*58*). We observe no such temperature dependence; without such an observation, the possibility of a bridge complex must be questioned.

DISCUSSION

Affinity of Cu^{2+} for Monomeric and Fibrillar Aβ. Despite a range of studies linking Cu^{2+} with Aβ neurotoxicity, a role for Cu^{2+} ions in the etiology of Alzheimer's disease has often been met with some scepticism; a common objection has been the relatively low affinity of Cu^{2+} for Aβ. Typically micromolar, and at most nanomolar, K_d values are reported (*44*−*46*, *59*). Our re-evaluation of the affinity of Cu^{2+} for Aβ places the K_d 2 or 3 orders of magnitude higher than previously believed. A picomolar affinity for Cu^{2+} now allows Aβ to compete for Cu^{2+} ions with other extracellular Cu^{2+} chelators, such as human serum albumin (HSA), particularly during neuronal depolarization; the biological significance of a picomolar affinity is discussed later.

We have used two independent methods of determining the affinity of Cu^{2+} for monomeric and fibrillar Aβ(1−42). The fluorescence quenching experiments show that both soluble and fibrillar Aβ(1−42) have identical affinities and are comparable to that of the Cu^{2+} chelator NTA (20 pM) for Cu^{2+} ions. There were some small differences in the affinities calculated depending on the competing ligand used (NTA, histidine, or glycine), but all three competitors exhibited affinities of Cu^{2+} for Aβ within less than 1 order of magnitude, placing the apparent (conditional) K_d between 6 and 60 pM at pH 7.4. We also used near-UV CD to monitor directly the location of Cu^{2+} ions competing between NTA or glycine and Aβ(1−28). Again, this indicated an affinity of Cu^{2+} for Aβ(1−28) comparable to that of NTA at pH 7.4. Glycine competition detected by fluorescence or near-UV CD revealed very similar affinities, validating the fluorescence quenching method.

We have considered the possibility that a ternary complex is formed among Cu^{2+}, Aβ, and the competing ligands NTA, L-histidine, and glycine (see, for example, refs *60* and *61*). However, we have a number of pieces of evidence that suggest this is unlikely. In particular, competition for Cu^{2+} ions between

Aβ and L-histidine detected by visible CD indicates that when sufficient (~4 molar equiv) L-histidine is added to the Cu^{2+}−Aβ complex a visible CD spectrum identical to that of $Cu(His)_2$ alone is observed. The visible CD spectra are very sensitive to Cu^{2+} coordination geometry, and the free $Cu(His)_2$ complex produces a characteristic visible CD spectrum with a positive CD band at 700 nm irrespective of the presence of Aβ, suggesting a ternary complex does not form (see Figure S6 of the Supporting Information). Furthermore, the Cu^{2+}-induced quenching of Tyr10 of Aβ almost completely returns upon addition of NTA (or other competing ligands). If Cu^{2+} remained bound to Aβ forming a ternary complex, one might expect some if not all of the Cu^{2+}-induced quenching to persist. In addition, the CD band at 320 nm attributed to the Cu^{2+}−Aβ imidazoles is completely lost with the addition of a competing ligand. If a ternary complex remained, one might expect the Cu^{2+}−imidazole band from the Cu^{2+}−Aβ complex also to be retained.

Previously reported affinities of Cu^{2+} for Aβ are only for the monomeric form. To the best of our knowledge, there are no Cu^{2+} affinity studies for Aβ fibrils. Garzon-Rodriguez et al. (*44*) found that Cu^{2+} had an affinity for monomeric Aβ(1−42) of ~2 μM. However, the Garzon-Rodriguez study was performed in Tris buffer, which has a weak but appreciable affinity for Cu^{2+} ions. This would have the effect of lowering the observed affinity. Two recent studies have shown that apparent K_d values reported in the literature of the Cu−Aβ complex, once corrected for coordination by Tris buffer, produce K_d values of 35 nM or 625 pM depending on the approach (*45*, *46*). Hatcher et al. suggest that as many as four stepwise Cu^{2+} dissociation constants must be considered for Tris buffer. Hatcher et al. also uses isothermal calorimetry (ITC) and determines an apparent dissociation constant of 0.4 nM for the Cu−Aβ complex at pH 7.4. This affinity is between 7 and 70 times weaker than that which we have determined here. The discrepancy might be explained by the use of high levels of Tris buffer as a competitor which might exaggerate systematic errors in the measurements. We and others have previously reported fluorescence quenching experiments and other completion studies using glycine in the absence of a buffer (*31*, *37*, *56*, *59*, *62*); however, Hatcher et al. have highlighted a failure to account for both of glycine's affinities. When the stepwise affinity, $K_{a1}K_{a2}$, for the $Cu(Gly)_2$ complex is used rather than simply K_{a1}, affinities comparable to those reported here may be calculated, as shown in Table 1.

The in-register stacking of successive monomeric units within fibers results in histidines at positions 13 and 14 aligning adjacent to each other along the length of the fibers (*63*, *64*); thus, groups of four histidine residues would be in the proximity of each other. We were particularly intrigued by the possibility that the very different affinities reported for the Cu−Aβ complex in the literature (K_d values between 10^{18} and 10^6) (*44*, *45*, *47*) might reflect differences in the Aβ oligomeric form studied. Importantly, we report no difference in affinity between monomeric and fibrillar Aβ. It now seems clear that the attomolar dissociation constant proposed by Atwood et al. (*47*) is out of line with other measurements and cannot be explained by the oligomeric state of Aβ.

Cu^{2+} Binding to Fibrils. Fibrils, once formed, retain their structure with Cu^{2+} additions, as judged by our UV CD and unperturbed ThT binding, but also by TEM (*41*). In agreement with previous studies (*41*), our EPR spectra suggest that the fibrillar Aβ−Cu^{2+} complex forms the same coordination geometry and ligands as monomeric Aβ. This is strongly supported by our observations that the affinity of Cu^{2+} for the two Aβ forms is almost identical. Interestingly, Aβ fibers are able to accommodate a full stoichiometric complement of Cu^{2+} ions; Cu^{2+} ions are able to diffuse into all parts of the fiber, giving precisely a 1:1 stoichiometry. The nature of the ligand's coordination geometry and pH dependence is discussed later but is shown in Figure 10. Our data do not suggest an intermolecular Cu−Aβ complex for the fibrillar form of Aβ.

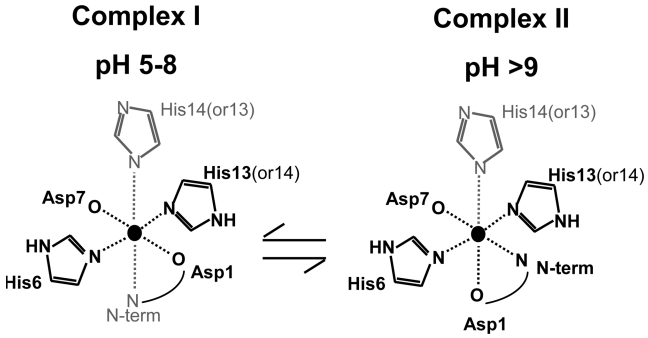

FIGURE 10: Proposed model of high-affinity binding of Cu^{2+} to Aβ(1−42) in both fibrillar and monomeric form. Complex I dominates at pH < 9. Coordinating ligands include all three histidine imidazole nitrogens but with two histidine ligands in the equatorial plane and a third axial. In addition, the N-terminal amino group coordinates at pH 7.4 as well as pH 9, but as an axial ligand at pH 7.4. The oxygen ligands are likely to arise from carboxylates; Asp1 and Asp7 are possibilities. At room temperature, the Cu^{2+} complex may be quite dynamic, exchanging between ligands in the equatorial and axial plane; without crystallographic data, this proposed coordination geometry is tentative. A second Cu^{2+} ion binds to Aβ at 2 molar equiv, and it is likely this complex is rich in carboxylate ligands.

Karr et al. have reported Cu^{2+} EPR spectra of fibrils for the low-pH species similar to those we have observed (*41*, *65*). However, they also argue on the basis of the solid state NMR models of Aβ fibers, that both His13 and His14 cannot bind a single Cu^{2+} ion in Aβ(1−40) because the β-sheet structure would be disrupted by the simultaneous coordination of two adjacent residues (*65*). However, we have shown that the Cu^{2+} affinity is the same in the fibers as in the monomers, which would be unlikely if either His13 or His14 were not part of the complex. Indeed, deuterium exchange experiments indicate that stable hydrogen bonds are not present between residues 1 and 14, suggesting a more flexible picture of Aβ fibers up to and including residue His14 (*64*, *66*). This explains why the Cu^{2+} coordination geometry is unaffected by the formation of fibrils and can contain both His13 and His14.

The β-sheet plane has been shown to be 4.7 Å apart in adjacent sheets (*67*). This, on average, would place adjacent His residues 4.7 Å apart. We see that Aβ can bind up to 1 molar equiv of Cu^{2+} ions. Dipolar through-space interactions of Cu^{2+} ions are typically felt between Cu^{2+} ions that are ≤7 Å apart and usually result in broadened spectra. It is therefore perhaps a surprise that some broadening of the EPR spectra is not observed, although it is certainly possible that the broadening is too small to be detected, although models of Cu^{2+}−Aβ fibers could be envisaged in which Cu^{2+} ions bound to His13 and His14 but remain more than 7 Å apart.

Coordination Geometry. cw-EPR suggests two pH-dependent species are formed with square-planar or tetragonal geometry. On the basis of $g_{\|}$ and hyperfine splitting values, complex I (at low pH) is composed of 2N2O or 3N1O ligands while complex II (at high pH) gives EPR spectra more typical of a complex with 3N1O or 4N ligands. We have used a range of Aβ analogues

to further probe the nature of the coordination geometry. It is commonly believed that all three histidines within Aβ form equatorial imidazole nitrogen ligands with the Cu^{2+} ion (*35*). It is therefore surprising that upon replacement of His6, His13, or His14 with alanine there is not a more significant effect on the appearance of the EPR spectra, as alternative imidazole nitrogens are not available to compensate for the alanine substitution. In contrast, removal of His6, His13, His14, or N-terminal acetylation reduces affinity for Cu^{2+} (Table 1) and in addition causes perturbed Cu^{2+}-loaded UV CD spectra compared to the Cu^{2+} wild-type spectra (*31*). It is notable that the H6A analogue has the most reduced affinity for Cu^{2+} followed by the N-terminus, while the affinity reduction observed for H13A or H14A is much less marked. To explain these seemingly conflicting observations, we suggest the EPR spectrum attributed to complex I is actually the result of a superposition of a mixture of species containing only two histidine ligands in the equatorial plane with a third histidine in the axial position. One of the histidine residues, or the N-terminal amino coordination, from the equatorial plane is replaced by the histidine that had originally occupied an axial position. We suggest that at room temperature it might be more appropriate to think of the Cu^{2+} complex as quite dynamic with two histidines in the equatorial plane and a third histidine axially coordinating, exchanging between each other, as shown in Figure 10. We note that without crystallographic data our proposed coordination geometry is only a tentative model of the Cu−Aβ complex. However, in support of the model, the EPR spectrum of Aβ(Ac10−16), which has only two potential nitrogen ligands in the equatorial plane, is similar in appearance to that of complex I.

The presence of axial ligands contributing to the tetragonal Cu^{2+} complex has largely been ignored in the literature, as they have little influence on EPR spectra. However, axial ligands will stabilize the Cu^{2+} complex and affect main chain conformation and biophysical properties. A study using EXAFS supports the presence of axial ligands which indicates there are six nitrogen/oxygen ligands in the first coordination sphere of the Cu^{2+} complex rather than four (*39*).

We note that a very recent study using cw-EPR and ^{15}N-labeled His analogues together with HYSCORE-EPR presents some similarities with our model; their low-pH complex contains a mixture of species with only two of the three imidazoles coordinating in the equatorial plane (*36*). In this study, His6 is described as the anchor in this complex. Interestingly, we show the H6A analogue has the most significant reduction in affinity for Cu^{2+} ions (Table 1), which supports this assertion. Other conclusions drawn by Drew et al. for the equatorial ligands appear not to be compatible with our data, in particular, the lack of the inclusion of the N-terminal amino group in the high-pH complex (*36*). Our model of complex II is based on EPR spectra of the N-terminally acetylated peptide; this analogue will not form the high-pH complex. This strongly indicates that complex II involves coordination from the N-terminal amino group presumably within the equatorial binding plane, as shown in Figure 10.

The pK_a values of N-terminal amino groups are typically 8.0. The pH at which the N-terminal amino group deprotonates may match the formation of complex II (dominant at pH 9), particularly if the pK_a for the N-terminus of Aβ is slightly higher than is normally observed. A study by Karr and Szalai (*68*) found that replacement of Asp1 with Asn favored the formation of complex II. This might be explained by the stabilizing effect of the negative carboxylate of Asp1, which will increase the pK_a of the N-terminal amino group closer to pH 9 compared to an Asn side chain at the same position. It seems probable that the mutation of Asp to Asn promotes the change of the N-terminal amino coordination from an axial position to the equatorial plane, thus supporting our model of coordinating ligands shown in Figure 10.

Previous studies using visible CD at physiological pH and below indicate a lack of optical activity from the d−d transition of the Cu−Aβ complex (*31*), suggesting that backbone amide coordination does not exist (*69*, *70*). However, increasing the pH above 8.5 may promote amide deprotonation and allows coordination of Cu^{2+} to the main chain, resulting in a CD band being observed at 520 nm (*31*). We suggest that the appearance of the CD band at 520 nm is due to coordination from the N-terminal amino group in the equatorial plane rather than from a main chain amide.

There is much debate in the literature about the source of the oxygen ligand in the equatorial plane; water is a possibility, but Karr and Szalai found that substituting $H_2^{17}O$ for $H_2^{16}O$ did not affect hyperfine splitting in their spectra, suggesting that water is not an equatorial ligand to Cu^{2+} in Aβ(1−40). The Tyr10 hydroxyl group has previously been suggested (*71*) as a ligand but has since been shown to be unlikely by ^1H NMR (*31*) which shows no significant broadening of the tyrosine ring protons. This is also supported by a lack of Cu^{2+} charge transfer bands associated with Cu-Tyr (*37*, *59*). Carbonyl main chain Cu^{2+} coordination is also a possibility; however, coordination of oxygen from one of the four carboxyl side chains (Asp1, Glu3, Asp7, and Glu11) in the first 16 residues is most probable. Karr et al. showed that the EPR spectra for D1N and E3Q analogues left complex 1 unchanged (*68*), although removal of Asp1 might simply result in it being replaced with an alternative carboxylate ligand which would give a very similar EPR spectrum. Asp1 and Asp7 (adjacent to His6) are our favored potential oxygen ligands for complex I, as shown in Figure 10. This is because the His6Ala analogue is more destabilized than the other analogues (see Figure 5 for the pH dependence and Table 1 for affinities), and coordination of the carboxyl and N-terminal amino group of Asp1 will form a stable six-membered chelate ring with the Cu^{2+} ion. A very recent study using ^{13}C-labeled Asp1 and HYSCORE-EPR suggested Asp1 carboxylate coordination in the low-pH complex (*36*).

Ab initio molecular modeling of the His13−His14 Cu^{2+} binding site suggests a trans arrangement of the two imidazole rings with a main chain carbonyl of His13 coordinating between the two His residues (*72*, *73*). However, this type of complex is likely to generate appreciable d−d transition signals which are not observed by CD (*31*). In contrast, a crystal structure of a model compound containing a dipeptide analogue of two adjacent histidine residues has been reported (*74*). In this compound, Cu^{2+} chelates to the εN atom of both imidazole rings, making a cis arrangement rather than trans coordination (90° rather than 180°) to the Cu^{2+} ion in a square-planar arrangement. Sterically, this type of ligand arrangement could facilitate the coordination of the N-terminus and His6 without any obvious restrictions but would stop main chain coordination to Cu^{2+}, as implied by the lack of a visible CD signal from d−d transitions, lending support to our proposed model shown in Figure 10.

Stoichiometry and the Second Binding Site. It is well established that two Cu^{2+} ions bind to fragments Aβ(1−16) and Aβ(1−28) (*31*, *56*). It was therefore surprising that the longer full-length Aβ binds only 1 molar equiv of Cu^{2+} ions with appreciable affinity, with a clear break point and saturation of the signal at 1 molar equiv (at 50 μM peptide). The difference between Aβ(1−28) and Aβ(1−42) is the 14 additional residues in the hydrophobic tail of Aβ(1−42); however, the two potential Cu^{2+} binding sites are in the first 16 residues. A possible explanation for the decreased binding stoichiometry of Aβ(1−42) compared to that of Aβ(1−28) may be hindrance to the second Cu^{2+} binding site by the hydrophobic tail in Aβ(1−42). To test this hypothesis, we wanted to disrupt intramolecular hydrophobic interactions. Alcohols, such as methanol, are thought to disrupt tertiary interactions and allow local interactions (hydrogen bonding) to dominate within the polypeptide chain (*75*). After addition of 20% (v/v) methanol, Aβ(1−42) bound a second Cu^{2+} ion as seen for the shorter Aβ(1−28).

In agreement with this study (in the absence of methanol), others have indicated a 1:1 stoichiometry for Aβ(1−40) (*44*, *45*). In contrast, a recent study reported that Aβ(1−40) can bind two Cu^{2+} ions (*47*). However, for this study, a cryoprotectant [50% (v/v) glycerol] was used. This alcohol (a triol), like methanol, is known to weaken hydrophobic interaction and promote intermolecular hydrogen bonding (*76*). Thus, the glycerol has the same effect as we have shown for 20% (v/v) methanol and explains the discrepancy in the stoichiometies reported.

The nature of the second Cu^{2+} binding site is not well-understood. It is clear that it is contained within the first 16 amino acids (*31*). EPR suggests that this binding site is also tetragonal or square-planar with the $A_{\|}$ and $g_{\|}$ values shifted to values more typical for oxygen than nitrogen ligands, perhaps 3O1N. We suggest that the first equivalent of Cu^{2+} binds to all three histidine residues, although one His is probably an axial ligand. It is notable that as the second molar equivalent of Cu^{2+} is added the binding mode of the first equivalent does not appear to be perturbed. It is therefore likely that the second mode of binding is rich in carboxylate ligands (D1, E3, D7, and E11) and perhaps a single nitrogen ligand, the N-terminus or His13/His14. Support for this comes from comparison of the EPR spectra of Aβ(1−11), which contains two potential nitrogen ligands. This fragment reveals a spectrum very different from that of the second molar equivalent spectrum of Aβ(1−28). Thus, this suggests a complex containing the N-terminus and His6 can be ruled out for the second weak binding site on Aβ. The affinity of the second molar equivalent has been determined to be 10^{-5} M (*59*).

Biological Significance. It seems clear that Aβ fibers once formed are able to accommodate the coordination of Cu^{2+} ions. Indeed, Cu^{2+} ions are found concentrated within amyloid plaques bound directly to Aβ (*7*, *8*). The affinity, coordination geometry, and stoichiometry are unaffected by the form of Aβ, monomeric or fibrillar. In particular, Aβ fibrils are able to accommodate a full stoichiometric complement of Cu^{2+} ions, and the β-sheet secondary structure is unperturbed.

Our data suggest Cu^{2+} ions are not involved in Aβ cross-linking within fibers. Cu^{2+} is certainly able to bind Aβ fibers once formed; less well understood is the potential effect Cu^{2+} has on inducing fiber formation. It is well established that in vitro Cu^{2+} significantly reduces the solubility of Aβ (*19*, *20*, *24*, *77*) but induces the formation of only amorphous aggregates rather than amyloids (*22*, *23*). It remains to be established what the effect of Cu^{2+} ions is on the rate of formation of fibers and diffusible Aβ oligomers in vivo. It is known that Cu^{2+} homeostasis within the brain is impaired in AD patients (*4*, *5*). It is possible that increasing Cu^{2+} levels may promote Aβ oligomerization and Cu^{2+}-loaded fibers may be more resistant to clearance, thus explaining the elevated level of Cu^{2+} ions in amyloid plaques (*6*, *8*).

Cu^{2+}-induced oxidative stress may also cause upregulation of Aβ as an antioxidant response (*13*, *78*), and this has led to a modified amyloid cascade hypothesis (*13*, *14*). The mechanism by which Aβ oligomers and fibers are toxic to neuronal cells is not well-established, although toxicity seems to be regulated by H_2O_2 (*12*). The most likely source of H_2O_2 and hydroxyl radicals is redox cycling of Cu^{2+} ions (*9*), induced by the physiological levels of extracellular ascorbate (*13*). It is well established that Cu^{2+} ions will bind to Aβ (monomeric and fibrillar) in a redox-active form (*13*, *15*, *79*, *80*). Indeed, an important study has recently shown that transfer of Cu^{2+} from Aβ to the redox-inactive metallothionein-3 removes Aβ's neurotoxic properties (*16*). Diffusible oligomers of Aβ could direct Cu^{2+} ions to the neuronal cell surface where Cu^{2+} would generate hydrogen peroxide and hydroxyl radicals. Indeed, Aβ oligomers are found clustered at synaptic termini (*81*) and cause memory loss due to synapse failure (*3*). Redox-active copper ions clustered at synaptic terminals will cause lipid peroxidation at the cell membrane and so compromise cell integrity (*13*, *15*), leading to the neuron loss characteristic of Alzheimer's disease.

The Cu^{2+} affinity reported here for Aβ(1−42) with an apparent (conditional) dissociation constant at pH 7.4 between 6 and 60 pM is a number of orders of magnitude greater than values in recent reports. This affinity is considerably greater than the extracellular Cu^{2+} concentration within cerebrospinal fluid (CSF) and extracellular brain interstitial fluid, which is typically 250 nM (*82*, *83*). Furthermore, levels of Cu^{2+} are found to be as much as 1000 times higher at the synapse (*6*) and within plaques (*6*, *84*). Although serum albumin is at lower levels in the CSF than blood plasma, at 3 μM, much of the Cu^{2+} is still likely to be bound to serum albumin, which has a K_d of 1.0 pM for Cu^{2+} ions at pH 7.4 (*85*, *86*). However, it is notable that the difference in affinity between albumin and Aβ is only a single order of magnitude. Additionally, at the synaptic cleft, fluxes of Cu^{2+} ions may be as high as 250 μM during neuronal depolarization (*ref84*) which is 2 orders of magnitude higher than the concentration of albumin. In these instances, albumin, and other copper binding proteins such as metallothionein-3, would be saturated with Cu^{2+} ions. Aβ, which is released from neuronal cells at the synapse (*81*), would therefore be able to bind fluxes of Cu^{2+} released during cellular depolarization. This higher affinity also has implications for the current interest in Cu^{2+} chelators, which have shown some efficacy as a treatment for AD (*26*−*28*). Potential chelators should have an affinity for Cu^{2+} 1 order of magnitude higher than that of Aβ, placing an ideal affinity at 10^{12} M^{-1}, comparable to that of human serum albumin.

Our studies have made a significant contribution to understanding Cu^{2+} coordination and affinity in both monomeric and fibrillar form. The re-evaluation of the affinity of Cu^{2+} for Aβ to picomolar levels adds weight to Cu^{2+} playing a central role in the formation of fibers, as well as the neurotoxic effects of redox-active Cu^{2+} ions bound to diffusible Aβ oligomers.

ACKNOWLEDGMENT

We thank John Nield for help with the TEM of Aβ fibers.

SUPPORTING INFORMATION AVAILABLE

Six figures showing (1) electron microscopy image of fibrils and ThT fibril growth curve of seeded and nonseeded amyloid-β peptide, (2) calculations for dissociation constants, (3) pH dependence of Aβ(1−28), (4) Aβ(1−42) with 20% (v/v) methanol, (5) temperature dependence of Aβ(1−28), and (6) visible CD spectra of Cu(L-histidine)$_2$ with Aβ(1−42) present. This material is available free of charge via the Internet at http://pubs.acs.org.

REFERENCES

1. Hardy, J., and Selkoe, D. J. (2002) The amyloid hypothesis of Alzheimer's disease: Progress and problems on the road to therapeutics. *Science 297*, 353–356.
2. Selkoe, D. J. (1996) Amyloid β-protein and the genetics of Alzheimer's disease. *J. Biol. Chem. 271*, 18295–18298.
3. Walsh, D. M., Klyubin, I., Fadeeva, J. V., Cullen, W. K., Anwyl, R., Wolfe, M. S., Rowan, M. J., and Selkoe, D. J. (2002) Naturally secreted oligomers of amyloid β protein potently inhibit hippocampal long-term potentiation in vivo. *Nature 416*, 535–539.
4. Cuajungco, M. P., and Lees, G. J. (1997) Zinc and Alzheimer's disease: Is there a direct link?. *Brain Res. Brain Res. Rev. 23*, 219–236.
5. Bush, A. I. (2003) The metallobiology of Alzheimer's disease. *Trends Neurosci. 26*, 207–214.
6. Lovell, M. A., Robertson, J. D., Teesdale, W. J., Campbell, J. L., and Markesbery, W. R. (1998) Copper, iron and zinc in Alzheimer's disease senile plaques. *J. Neurol. Sci. 158*, 47–52.
7. Dong, J., Atwood, C. S., Anderson, V. E., Siedlak, S. L., Smith, M. A., Perry, G., and Carey, P. R. (2003) Metal binding and oxidation of amyloid-β within isolated senile plaque cores: Raman microscopic evidence. *Biochemistry 42*, 2768–2773.
8. Miller, L. M., Wang, Q., Telivala, T. P., Smith, R. J., Lanzirotti, A., and Miklossy, J. (2006) Synchrotron-based infrared and X-ray imaging shows focalized accumulation of Cu and Zn co-localized with β-amyloid deposits in Alzheimer's disease. *J. Struct. Biol. 155*, 30–37.
9. Opazo, C., Huang, X., Cherny, R. A., Moir, R. D., Roher, A. E., White, A. R., Cappai, R., Masters, C. L., Tanzi, R. E., Inestrosa, N. C., and Bush, A. I. (2002) Metalloenzyme-like activity of Alzheimer's disease β-amyloid. Cu-dependent catalytic conversion of dopamine, cholesterol, and biological reducing agents to neurotoxic H_2O_2. *J. Biol. Chem. 277*, 40302–40308.
10. Gaggelli, E., Kozlowski, H., Valensin, D., and Valensin, G. (2006) Copper homeostasis and neurodegenerative disorders (Alzheimer's, prion, and Parkinson's diseases and amyotrophic lateral sclerosis). *Chem. Rev. 106*, 1995–2044.
11. Butterfield, D. A., Reed, T., Newman, S. F., and Sultana, R. (2007) Roles of amyloid β-peptide-associated oxidative stress and brain protein modifications in the pathogenesis of Alzheimer's disease and mild cognitive impairment. *Free Radical Biol. Med. 43*, 658–677.
12. Behl, C., Davis, J. B., Lesley, R., and Schubert, D. (1994) Hydrogen peroxide mediates amyloid β protein toxicity. *Cell 77*, 817–827.
13. Nadal, R. C., Rigby, S. E., and Viles, J. H. (2008) Amyloid β-Cu^{2+} complexes in both monomeric and fibrillar forms do not generate H_2O_2 catalytically but quench hydroxyl radicals. *Biochemistry 47*, 11653–11664.
14. Lee, H. G., Zhu, X., Castellani, R. J., Nunomura, A., Perry, G., and Smith, M. A. (2007) Amyloid-β in Alzheimer disease: The null versus the alternate hypotheses. *J. Pharmacol. Exp. Ther. 321*, 823–829.
15. Murray, I. V., Sindoni, M. E., and Axelsen, P. H. (2005) Promotion of oxidative lipid membrane damage by amyloid β proteins. *Biochemistry 44*, 12606–12613.
16. Meloni, G., Sonois, V., Delaine, T., Guilloreau, L., Gillet, A., Teissie, J., Faller, P., and Vasak, M (2008) Metal swap between Zn7-metallothionein-3 and amyloid-β-Cu protects against amyloid-β toxicity. *Nat. Chem. Biol. 4*, 366–372.
17. Lambert, M. P., Barlow, A. K., Chromy, B. A., Edwards, C., Freed, R., Liosatos, M., Morgan, T. E., Rozovsky, I., Trommer, B., Viola, K. L., Wals, P., Zhang, C., Finch, C. E., Krafft, G. A., and Klein, W. L. (1998) Diffusible, nonfibrillar ligands derived from Aβ1−42 are potent central nervous system neurotoxins. *Proc. Natl. Acad. Sci. U. S.A. 95*, 6448–6453.
18. Vigo-Pelfrey, C., Lee, D., Keim, P., Lieberburg, I., and Schenk, D. B. (1993) Characterization of β-amyloid peptide from human cerebrospinal fluid. *J. Neurochem. 61*, 1965–1968.
19. Bush, A. I., Pettingell, W. H., Multhaup, G., d Paradis, M., Vonsattel, J. P., Gusella, J. F., Beyreuther, K., Masters, C. L., and Tanzi, R. E. (1994) Rapid induction of Alzheimer A β amyloid formation by zinc. *Science 265*, 1464–1467.
20. Atwood, C. S., Moir, R. D., Huang, X., Scarpa, R. C., Bacarra, N. M., Romano, D. M., Hartshorn, M. A., Tanzi, R. E., and Bush, A. I. (1998) Dramatic aggregation of Alzheimer Aβ by Cu(II) is induced by conditions representing physiological acidosis. *J. Biol. Chem. 273*, 12817–12826.
21. Atwood, C. S., Perry, G., Zeng, H., Kato, Y., Jones, W. D., Ling, K. Q., Huang, X., Moir, R. D., Wang, D., Sayre, L. M., Smith, M. A., Chen, S. G., and Bush, A. I. (2004) Copper mediates dityrosine cross-linking of Alzheimer's amyloid-β. *Biochemistry 43*, 560–568.
22. Yoshiike, Y., Tanemura, K., Murayama, O., Akagi, T., Murayama, M., Sato, S., Sun, X., Tanaka, N., and Takashima, A. (2001) New insights on how metals disrupt amyloid β-aggregation and their effects on amyloid-β cytotoxicity. *J. Biol. Chem. 276*, 32293–32299.
23. Raman, B., Ban, T., Yamaguchi, K., Sakai, M., Kawai, T., Naiki, H., and Goto, Y. (2005) Metal ion-dependent effects of clioquinol on the fibril growth of an amyloid β peptide. *J. Biol. Chem. 280*, 16157–16162.
24. Huang, X., Atwood, C. S., Moir, R. D., Hartshorn, M. A., Tanzi, R. E., and Bush, A. I. (2004) Trace metal contamination initiates the apparent auto-aggregation, amyloidosis, and oligomerization of Alzheimer's Aβ peptides. *J. Biol. Inorg. Chem. 9*, 954–960.
25. Cherny, R. A., Legg, J. T., McLean, C. A., Fairlie, D. P., Huang, X., Atwood, C. S., Beyreuther, K., Tanzi, R. E., Masters, C. L., and Bush, A. I. (1999) Aqueous dissolution of Alzheimer's disease Aβ amyloid deposits by biometal depletion. *J. Biol. Chem. 274*, 23223–23228.
26. Cherny, R. A., Atwood, C. S., Xilinas, M. E., Gray, D. N., Jones, W. D., McLean, C. A., Barnham, K. J., Volitakis, I., Fraser, F. W., Kim, Y., Huang, X., Goldstein, L. E., Moir, R. D., Lim, J. T., Beyreuther, K., Zheng, H., Tanzi, R. E., Masters, C. L., and Bush, A. I. (2001) Treatment with a copper-zinc chelator markedly and rapidly inhibits β-amyloid accumulation in Alzheimer's disease transgenic mice. *Neuron 30*, 665–676.
27. Bush, A. I. (2002) Metal complexing agents as therapies for Alzheimer's disease. *Neurobiol. Aging 23*, 1031–1038.
28. Ritchie, C. W., Bush, A. I., Mackinnon, A., Macfarlane, S., Mastwyk, M., MacGregor, L., Kiers, L., Cherny, R., Li, Q. X., Tammer, A., Carrington, D., Mavros, C., Volitakis, I., Xilinas, M., Ames, D., Davis, S., Beyreuther, K., Tanzi, R. E., and Masters, C. L. (2003) Metal-protein attenuation with iodochlorhydroxyquin (clioquinol) targeting Aβ amyloid deposition and toxicity in Alzheimer disease: A pilot phase 2 clinical trial. *Arch. Neurol. 60*, 1685–1691.
29. Sparks, D. L., and Schreurs, B. G. (2003) Trace amounts of copper in water induce β-amyloid plaques and learning deficits in a rabbit model of Alzheimer's disease. *Proc. Natl. Acad. Sci. U.S.A. 100*, 11065–11069.
30. Marx, J. (2003) Neuroscience. Possible role for environmental copper in Alzheimer's disease. *Science 301*, 905.
31. Syme, C. D., Nadal, R. C., Rigby, S. E., and Viles, J. H. (2004) Copper binding to the amyloid-β (Aβ) peptide associated with Alzheimer's disease: Folding, coordination geometry, pH dependence, stoichiometry, and affinity of Aβ-(1−28): Insights from a range of complementary spectroscopic techniques. *J. Biol. Chem. 279*, 18169–18177.
32. Syme, C. D., and Viles, J. H. (2006) Solution ^{1}H NMR investigation of Zn^{2+} and Cd^{2+} binding to amyloid-β peptide (Aβ) of Alzheimer's disease. *Biochim. Biophys. Acta 1764*, 246–256.
33. Brown, D. R., and Kozlowski, H. (2004) Biological inorganic and bioinorganic chemistry of neurodegeneration based on prion and Alzheimer diseases. *Dalton Trans.,* 1907–1917.
34. Faller, P., and Hureau, C. (2009) Bioinorganic chemistry of copper and zinc ions coordinated to amyloid-β peptide. *Dalton Trans.,* 1080–1094.
35. Shin, B. K., and Saxena, S. (2008) Direct evidence that all three histidine residues coordinate to Cu(II) in amyloid-β1−16. *Biochemistry 47*, 9117–9123.
36. Drew, S. C., Noble, C. J., Masters, C. L., Hanson, G. R., and Barnham, K. J. (2009) Pleomorphic copper coordination by Alzheimer's disease amyloid-β peptide. *J. Am. Chem. Soc. 131*, 1195–1207.
37. Kowalik-Jankowska, T., Ruta, M., Wisniewska, K., and Lankiewicz, L. (2003) Coordination abilities of the 1−16 and 1−28 fragments of β-amyloid peptide towards copper(II) ions: A combined potentiometric and spectroscopic study. *J. Inorg. Biochem. 95*, 270–282.
38. Damante, C. A., Osz, K., Nagy, Z., Pappalardo, G., Grasso, G., Impellizzeri, G., Rizzarelli, E., and Sovago, I. (2008) The Metal Loading Ability of β-Amyloid N-Terminus: A Combined Potentiometric and Spectroscopic Study of Copper(II) Complexes with β-Amyloid(1−16), Its Short or Mutated Peptide Fragments, and Its Polyethylene Glycol (PEG)-ylated Analogue. *Inorg. Chem. 47*, 9669–9683.

39. Streltsov, V. A., SJ, J. T., Epa, V. C., Barnham, K. J., Masters, C. L., and Varghese, J. N. (2009) The structure of the amyloid β-peptide high affinity copper II binding site in Alzheimer's disease. *Biophys. J. 95*, 3447–3456.
40. Hou, L., and Zagorski, M. G. (2006) NMR reveals anomalous copper (II) binding to the amyloid Aβ peptide of Alzheimer's disease. *J. Am. Chem. Soc. 128*, 9260–9261.
41. Karr, J. W., and Szalai, V. A. (2008) Cu(II) binding to monomeric, oligomeric, and fibrillar forms of the Alzheimer's disease amyloid-β peptide. *Biochemistry 47*, 5006–5016.
42. Antzutkin, O. N. (2004) Amyloidosis of Alzheimer's Aβ peptides: Solid-state nuclear magnetic resonance, electron paramagnetic resonance, transmission electron microscopy, scanning transmission electron microscopy and atomic force microscopy studies. *Magn. Reson. Chem. 42*, 231–246.
43. Petkova, A. T., Ishii, Y., Balbach, J. J., Antzutkin, O. N., Leapman, R. D., Delaglio, F., and Tycko, R. (2002) A structural model for Alzheimer's β-amyloid fibrils based on experimental constraints from solid state NMR. *Proc. Natl. Acad. Sci. U.S.A. 99*, 16742–16747.
44. Garzon-Rodriguez, W., Yatsimirsky, A. K., and Glabe, C. G. (1999) Binding of Zn(II), Cu(II), and Fe(II) ions to Alzheimer's A β peptide studied by fluorescence. *Bioorg. Med. Chem. Lett. 9*, 2243–2248.
45. Tougu, V., Karafin, A., and Palumaa, P. (2008) Binding of zinc(II) and copper(II) to the full-length Alzheimer's amyloid-β peptide. *J. Neurochem. 104*, 1249–1259.
46. Hatcher, L. Q., Hong, L., Bush, W. D., Carducci, T., and Simon, J. D. (2008) Quantification of the binding constant of copper(II) to the amyloid-β peptide. *J. Phys. Chem. B 112*, 8160–8164.
47. Atwood, C. S., Scarpa, R. C., Huang, X., Moir, R. D., Jones, W. D., Fairlie, D. P., Tanzi, R. E., and Bush, A. I. (2000) Characterization of copper interactions with alzheimer amyloid β peptides: Identification of an attomolar-affinity copper binding site on amyloid β1−42. *J. Neurochem. 75*, 1219–1233.
48. Gill, S. C., and von Hippel, P. H. (1989) Calculation of protein extinction coefficients from amino acid sequence data. *Anal. Biochem. 182*, 319–326.
49. Peisach, J., and Blumberg, W. E. (1974) Structural implications derived from the analysis of electron paramagnetic resonance spectra of natural and artificial copper proteins. *Arch. Biochem. Biophys. 165*, 691–708.
50. Dawson, R. M. C., Elliot, D. C., Elliot, W. H., and Jones, K. M. ((1986)) *Data for Biochemical Research*, Claredon Press, Oxford, U.K..
51. Wells, M. A., Jelinska, C., Hosszu, L. L., Craven, C. J., Clarke, A. R., Collinge, J., Waltho, J. P., and Jackson, G. S. (2006) Multiple forms of copper (II) co-ordination occur throughout the disordered N-terminal region of the prion protein at pH 7.4. *Biochem. J. 400*, 501–510.
52. Sieracki, N. A., Hwang, H. J., Lee, M. K., Garner, D. K., and Lu, Y. (2008) A temperature independent pH (TIP) buffer for biomedical biophysical applications at low temperatures. *Chem. Commun.,* 823–825.
53. Williams-Smith, D. L., Bray, R. C., Barber, M. J., Tsopanakis, A. D., and Vincent, S. P. (1977) Changes in apparent pH on freezing aqueous buffer solutions and their relevance to biochemical electron-paramagnetic-resonance spectroscopy. *Biochem. J. 167*, 593–600.
54. Naiki, H., Higuchi, K., Hosokawa, M., and Takeda, T. (1989) Fluorometric determination of amyloid fibrils in vitro using the fluorescent dye, thioflavin T1. *Anal. Biochem. 177*, 244–249.
55. Aronoff-Spencer, E., Burns, C. S., Avdievich, N. I., Gerfen, G. J., Peisach, J., Antholine, W. E., Ball, H. L., Cohen, F. E., Prusiner, S. B., and Millhauser, G. L. (2000) Identification of the Cu^{2+} binding sites in the N-terminal domain of the prion protein by EPR and CD spectroscopy. *Biochemistry 39*, 13760–13771.
56. Curtain, C. C., Ali, F., Volitakis, I., Cherny, R. A., Norton, R. S., Beyreuther, K., Barrow, C. J., Masters, C. L., Bush, A. I., and Barnham, K. J. (2001) Alzheimer's disease amyloid-β binds copper and zinc to generate an allosterically ordered membrane-penetrating structure containing superoxide dismutase-like subunits. *J. Biol. Chem. 276*, 20466–20473.
57. Smith, D. P., Smith, D. G., Curtain, C. C., Boas, J. F., Pilbrow, J. R., Ciccotosto, G. D., Lau, T. L., Tew, D. J., Perez, K., Wade, J. D., Bush, A. I., Drew, S. C., Separovic, F., Masters, C. L., Cappai, R., and Barnham, K. J. (2006) Copper-mediated amyloid-β toxicity is associated with an intermolecular histidine bridge. *J. Biol. Chem. 281*, 15145–15154.
58. Valentine, J. S., Pantoliano, M. W., McDonnell, P. J., Burger, A. R., and Lippard, S. J. (1979) pH-dependent migration of copper(II) to the vacant zinc-binding site of zinc-free bovine erythrocyte superoxide dismutase. *Proc. Natl. Acad. Sci. U.S.A. 76*, 4245–4249.
59. Guilloreau, L., Damian, L., Coppel, Y., Mazarguil, H., Winterhalter, M., and Faller, P. (2006) Structural and thermodynamical properties of CuII amyloid-β16/28 complexes associated with Alzheimer's disease. *J. Biol. Inorg. Chem. 11*, 1024–1038.
60. Rozga, M., Protas, A. M., Jablonowska, A., Dadlez, M., and Bal, W. (2009) The Cu(ii) complex of Aβ40 peptide in ammonium acetate solutions. Evidence for ternary species formation. *Chem. Commun.,* 1374–1376.
61. Burns, C. J., Field, L. D., Hambley, T. W., Lin, T., Ridley, D. D., Turner, P., and Wilkinson, M. P. (2001) X-ray crystal structural determination of copper(II)-nitrilotriacetic acid-bis(N-methylimidazol-2-yl)ketone ternary complex. *ARKIVOC (Zurich, Switz.) 7*, 157–165.
62. Ma, Q. F., Hu, J., Wu, W. H., Liu, H. D., Du, J. T., Fu, Y., Wu, Y. W., Lei, P., Zhao, Y. F., and Li, Y. M. (2006) Characterization of copper binding to the peptide amyloid-β(1−16) associated with Alzheimer's disease. *Biopolymers 83*, 20–31.
63. Tycko, R. (2004) Progress towards a molecular-level structural understanding of amyloid fibrils. *Curr. Opin. Struct. Biol. 14*, 96–103.
64. Whittemore, N. A., Mishra, R., Kheterpal, I., Williams, A. D., Wetzel, R., and Serpersu, E. H. (2005) Hydrogen-deuterium (H/D) exchange mapping of Aβ1−40 amyloid fibril secondary structure using nuclear magnetic resonance spectroscopy. *Biochemistry 44*, 4434–4441.
65. Karr, J. W., Akintoye, H., Kaupp, L. J., and Szalai, V. A. (2005) N-Terminal deletions modify the Cu^{2+} binding site in amyloid-β. *Biochemistry 44*, 5478–5487.
66. Olofsson, A., Lindhagen-Persson, M., Sauer-Eriksson, A. E., and Ohman, A. (2007) Amide solvent protection analysis demonstrates that amyloid-β(1−40) and amyloid-β(1−42) form different fibrillar structures under identical conditions. *Biochem. J. 404*, 63–70.
67. Serpell, L. C. (2000) Alzheimer's amyloid fibrils: Structure and assembly. *Biochim. Biophys. Acta 1502*, 16–30.
68. Karr, J. W., and Szalai, V. A. (2007) Role of Aspartate-1 in Cu(II) Binding to the Amyloid-β Peptide of Alzheimer's Disease. *J. Am. Chem. Soc. 129*, 3796–3797.
69. Klewpatinond, M., Davies, P., Bowen, S., Brown, D. R., and Viles, J. H. (2008) Deconvoluting the Cu^{2+} binding modes of full-length prion protein. *J. Biol. Chem. 283*, 1870–1881.
70. Klewpatinond, M., and Viles, J. H. (2007) Empirical rules for rationalising visible circular dichroism of Cu^{2+} and Ni^{2+} histidine complexes: Applications to the prion protein. *FEBS Lett. 581*, 1430–1434.
71. Miura, T., Suzuki, K., Kohata, N., and Takeuchi, H. (2000) Metal binding modes of Alzheimer's amyloid β-peptide in insoluble aggregates and soluble complexes. *Biochemistry 39*, 7024–7031.
72. Raffa, D. F., Gomez-Balderas, R., Brunelle, P., Rickard, G. A., and Rauk, A. (2005) Ab initio model studies of copper binding to peptides containing a His-His sequence: Relevance to the β-amyloid peptide of Alzheimer's disease. *J. Biol. Inorg. Chem. 10*, 887–902.
73. Rauk, A. (2008) Why is the amyloid β peptide of Alzheimer's disease neurotoxic? *Dalton Trans.,* 1273–1282.
74. Hori, F., Kojima, Y., and Mastsumoto, K. (1979) The Synthesis and Crystal Structure of Bis(cyclo-L-histidyl-L-histidyl)copper(II) Perchlorate Tetrahydrate. *Bull. Chem. Soc. Jpn. 52*, 1076–1079.
75. Kony, D. B., Hunenberger, P. H., and van Gunsteren, W. F. (2007) Molecular dynamics simulations of the native and partially folded states of ubiquitin: Influence of methanol cosolvent, pH, and temperature on the protein structure and dynamics. *Protein Sci. 16*, 1101–1118.
76. Jones, D. T., Moody, C. M., Uppenbrink, J., Viles, J. H., Doyle, P. M., Harris, C. J., Pearl, L. H., Sadler, P. J., and Thornton, J. M. (1996) Towards meeting the Paracelsus Challenge: The design, synthesis, and characterization of paracelsin-43, an α-helical protein with over 50% sequence identity to an all-β protein. *Proteins 24*, 502–513.
77. Sengupta, P., Garai, K., Sahoo, B., Shi, Y., Callaway, D. J., and Maiti, S. (2003) The amyloid β peptide (Aβ(1−40)) is thermodynamically soluble at physiological concentrations. *Biochemistry 42*, 10506–10513.
78. Tamagno, E., Guglielmotto, M., Aragno, M., Borghi, R., Autelli, R., Giliberto, L., Muraca, G., Danni, O., Zhu, X., Smith, M. A., Perry, G., Jo, D. G., Mattson, M. P., and Tabaton, M. (2008) Oxidative stress activates a positive feedback between the γ- and β-secretase cleavages of the β-amyloid precursor protein. *J. Neurochem. 104*, 683–695.
79. Dikalov, S. I., Vitek, M. P., and Mason, R. P. (2004) Cupric-amyloid β peptide complex stimulates oxidation of ascorbate and generation of hydroxyl radical. *Free Radical Biol. Med. 36*, 340–347.
80. Guilloreau, L., Combalbert, S., Sournia-Saquet, A., Mazarguil, H., and Faller, P. (2007) Redox chemistry of copper-amyloid-β: The

generation of hydroxyl radical in the presence of ascorbate is linked to redox-potentials and aggregation state. *ChemBioChem 8*, 1317–1325.
81. Lacor, P. N., Buniel, M. C., Chang, L., Fernandez, S. J., Gong, Y., Viola, K. L., Lambert, M. P., Velasco, P. T., Bigio, E. H., Finch, C. E., Krafft, G. A., and Klein, W. L. (2004) Synaptic targeting by Alzheimer's-related amyloid β oligomers. *J. Neurosci. 24*, 10191–10200.
82. Joergstuerenburg, H., Oechsner, M., Schroeder, S., and Kunze, K. (1999) Determinants of the copper concentration in cerebrospinal fluid. *J. Neurol., Neurosurg. Psychiatry 67*, 252–253.
83. Ciba-Geigy ((1984)) *Physical Chemistry, Composition of Blood, Hematology, Somatometric Data*, 8th ed., Vol. *3*, Ciba-Geigy, Basel, Switzerland.
84. Kardos, J., Kovacs, I., Hajos, F., Kalman, M., and Simonyi, M. (1989) Nerve endings from rat brain tissue release copper upon depolarization. A possible role in regulating neuronal excitability. *Neurosci. Lett. 103*, 139–144.
85. Masuoka, J., Hegenauer, J., Van Dyke, B. R., and Saltman, P. (1993) Intrinsic stoichiometric equilibrium constants for the binding of zinc (II) and copper(II) to the high affinity site of serum albumin. *J. Biol. Chem. 268*, 21533–21537.
86. Rozga, M., Kloniecki, M., Jablonowska, A., Dadlez, M., and Bal, W. (2007) The binding constant for amyloid Aβ40 peptide interaction with human serum albumin. *Biochem. Biophys. Res. Commun. 364*, 714–718.